frontiers | Frontiers in Earth Science

TYPE Original Research
PUBLISHED 21 November 2024
DOI 10.3389/feart.2024.1487090

Early paleozoic evolution of the South Bainaimiao Ocean: constraints from the Chegendalai ophiolite mélange

Chenfei Feng, Guosheng Wang*, Zhiguang Zhou, Shen Gao, Jianfeng Chen and Hao Hu

School of Earth Sciences and Resources, China University of Geosciences, Beijing, Beijing, China

Check for updates

OPEN ACCESS

EDITED BY
Derek Keir,
University of Southampton, United Kingdom

REVIEWED BY
Junpeng Wang,
China University of Geosciences
Wuhan, China
Darko Spahić,
Institute for Multidisciplinary Research,
University of Belgrade, Serbia

*CORRESPONDENCE
Guosheng Wang,
wanggsh@cugb.edu.cn

RECEIVED 27 August 2024
ACCEPTED 31 October 2024
PUBLISHED 21 November 2024

CITATION
Feng C, Wang G, Zhou Z, Gao S, Chen J and Hu H (2024) Early paleozoic evolution of the South Bainaimiao Ocean: constraints from the Chegendalai ophiolite mélange.
Front. Earth Sci. 12:1487090.
doi: 10.3389/feart.2024.1487090

Introduction: Arc-continent collision contributes to the accretion of continental crust in the Central Asian Orogenic Belt. The Chegendalai ophiolitic mélange, located between the Bainaimiao arc and the North China Craton, is important to understanding the early Paleozoic evolution of the South Bainaimiao Ocean and arc-continent collision processes.

Methods: In this study, we provide Early Paleozoic geochronological and geochemical data from the Chegendalai ophiolitic mélange and island arc magmatic rocks in northern Damaoqi.

Results: Zircon U-Pb dating of ultrabasic rocks and diabase porphyrite from the Chegendalai ophiolitic mélange yielded ages of 424 Ma and 431.9 Ma, respectively. Schist has an age of 421 Ma. Zircon U-Pb ages of island arc magmatic rocks are 425.7 Ma for tonalite, and 431 $\pm$ 11 Ma and 433.2 $\pm$ 4.4 Ma for granodiorite. Gabbro and ultrabasic rocks were formed in a volcanic arc basalt or mid-ocean ridge setting, displaying a tholeiitic basalt signature. These rocks likely derived from the lithospheric mantle with assimilation of crustal materials. Intermediate-acid magmatic rocks in northern Damaoqi are geochemically classified as I-type granites and exhibit characteristics of adakites.

Discussion: These rocks formed by partial melting of subducted plates and interactions with crustal and mantle wedges in a volcanic arc setting. Based on these results, we propose a three-stage evolution model for the South Bainaimiao Ocean: (i) Initial subduction during the Ordovician (~450 Ma), where the Bainaimiao arc separated the South Bainaimiao Ocean from the PaleoAsian Ocean, with the former acting as a branch ocean basin of the latter; (ii) Northward subduction from the Ordovician to Late Silurian (450–424 Ma), with the South Bainaimiao Ocean subducting northward. The subducted slab partially melted and interacted with the crust-mantle wedge, leading to the formation of subduction-related island arc magmatic rocks; (iii) Closure during the Late Silurian (424–421 Ma), marked by the collision of the Bainaimiao arc with the North China Craton in an arc-continent collision, ending orogenesis with the Xibiehe Formation.

KEYWORDS

central asian orogenic belt (CAOB), south bainaimiao ocean, bainaimiao arc, arc-continent collision, ophiolitic mélange

1 Introduction

The Central Asian Orogenic Belt (CAOB), located between the Siberian Craton, the North China Craton (NCC), and the Tarim Craton, serves as a prototypical accretionary orogenic belt since the Phanerozoic (Figure 1A) (Şengör et al., 1993). The accretionary orogenic process of the CAOB elucidates crustal accretion mechanisms driven by plate tectonics, although its modes of accretion remain contentious (Şengör et al., 1993; Xiao et al., 2003; Windley et al., 2007; Safonova et al., 2011). Many researchers propose that the formation of the CAOB from the Neoproterozoic to Late Paleozoic can be explained by the models involving southwest Pacific-style island arc and microcontinent accretion (Xiao et al., 2003; Windley et al., 2007; Safonova et al., 2011; Kröner et al., 2014). Arc-continent collision is a major mechanism of crustal accretion in the western Pacific region (Brown et al., 2006; Whattam, 2009; Konstantinovskaya, 2011). Recent reports highlight Paleozoic arc-continent collision events in the southern Urals, Kazakhstan, and southern Mongolia within the CAOB (Alvarez-Marron et al., 2000; Brown et al., 2006; Degtyarev and Ryazantsev, 2007; Johnson et al., 2007; Li et al., 2023; Zeng et al., 2023), indicating that arc-continent collision is a crucial mechanism for continental crust growth and the formation of the CAOB (Şengör et al., 1993; Li, 2004; Yuan et al., 2009; Chen et al., 2021; Xiao et al., 2022; Li et al., 2023).

The southern margin of CAOB adjacent to the NCC is characterized by the Bainaimiao arc. Previous studies suggest that the Bainaimiao arc is an Andean-type active continental margin arc formed during the Early Paleozoic by the southward subduction of the Paleo-Asian Ocean beneath the NCC (Gu et al., 2012; Zhang et al., 2013; Wu et al., 2016; Ma et al., 2020). Recently, many researchers have proposed the existence of the South Bainaimiao Ocean between the Bainaimiao arc and the NCC prior to the late Silurian. Following the subduction of the South Bainaimiao Ocean, the Bainaimiao arc, as an allochthonous terrane, collided with and amalgamated into the NCC during the Late Silurian period (Li et al., 2012; Zhang et al., 2014; Li et al., 2015; Wang et al., 2016; Zhang et al., 2018; Zhou, H. et al., 2018; Ma et al., 2019; Chen et al., 2020; Hou et al., 2020; Liu et al., 2020; Ma et al., 2020; Alexis N'dri et al., 2021; Meng et al., 2021; Tang et al., 2021; Zhou et al., 2021; Li et al., 2023; Li et al., 2023; Li et al., 2023; Tian et al., 2023). Many studies have proposed the existence of the South Bainaimiao Ocean, but they differ its subduction polarity. Some argue that it subducted northward beneath the Bainaimiao arc, while the northern margin of the NCC remained in a passive continental margin stage (Zhang et al., 2014; Meng et al., 2021; Li et al., 2023; Zeng et al., 2023; Zhang et al., 2024); others propose that the Paleozoic Bainaimiao Ocean subducted southward beneath the northern margin of the NCC, influencing the Bainaimiao arc due to the southward subduction of the Paleo-Asian Ocean (Chen et al., 2018; Shi et al., 2024).

The Early Paleozoic ophiolitic mélanges of Chegendalai are situated between the Bainaimiao arc and the northern margin of the NCC. To the north, there is extensive development of early Paleozoic arc-related island arc magmatic rocks (Figure 2), making this area ideal for studying the evolution of the South Bainaimiao Ocean and the arc-continent collision (Zhang et al., 2014). This study conducted petrological, geochronological, and geochemical methods to analyze the formation ages and tectonic settings of the Chegendalai ophiolite mélange belt and the magmatic rocks in the

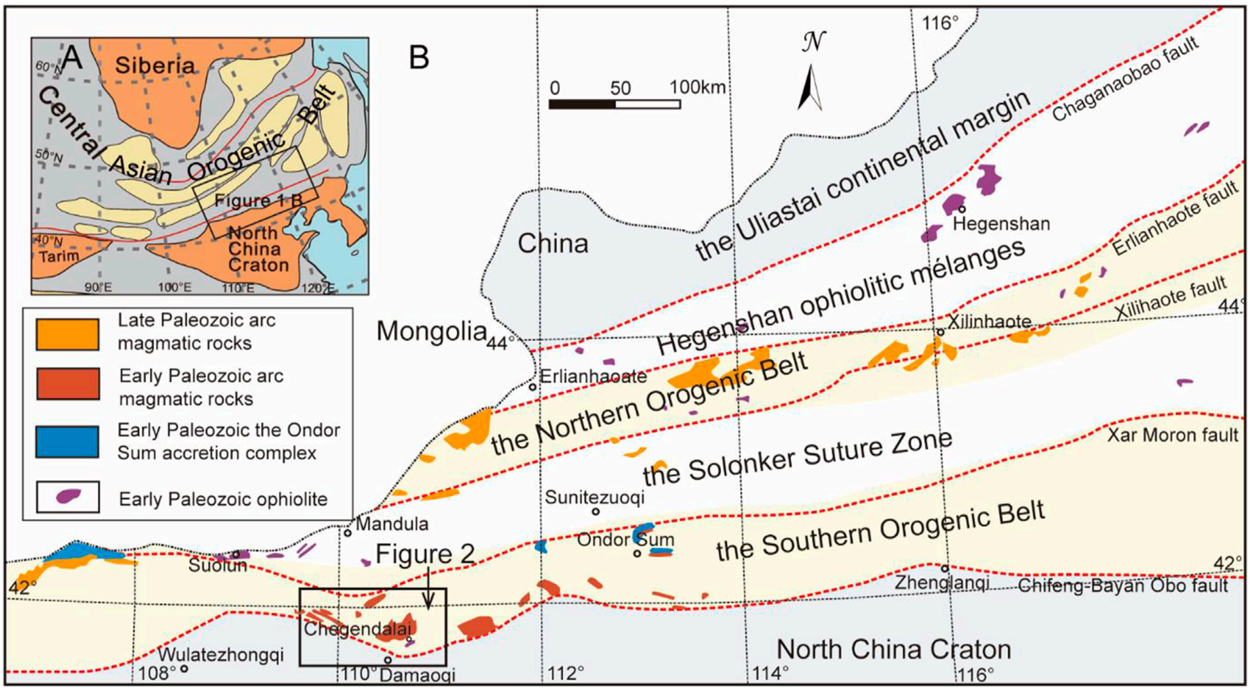

FIGURE 1
(A) The geotectonic location of the Central Asian orogenic belt (Hu et al., 2022); **(B)** Tectonic unit division of the XMOB (Xiao et al., 2003; Zhang et al., 2018).

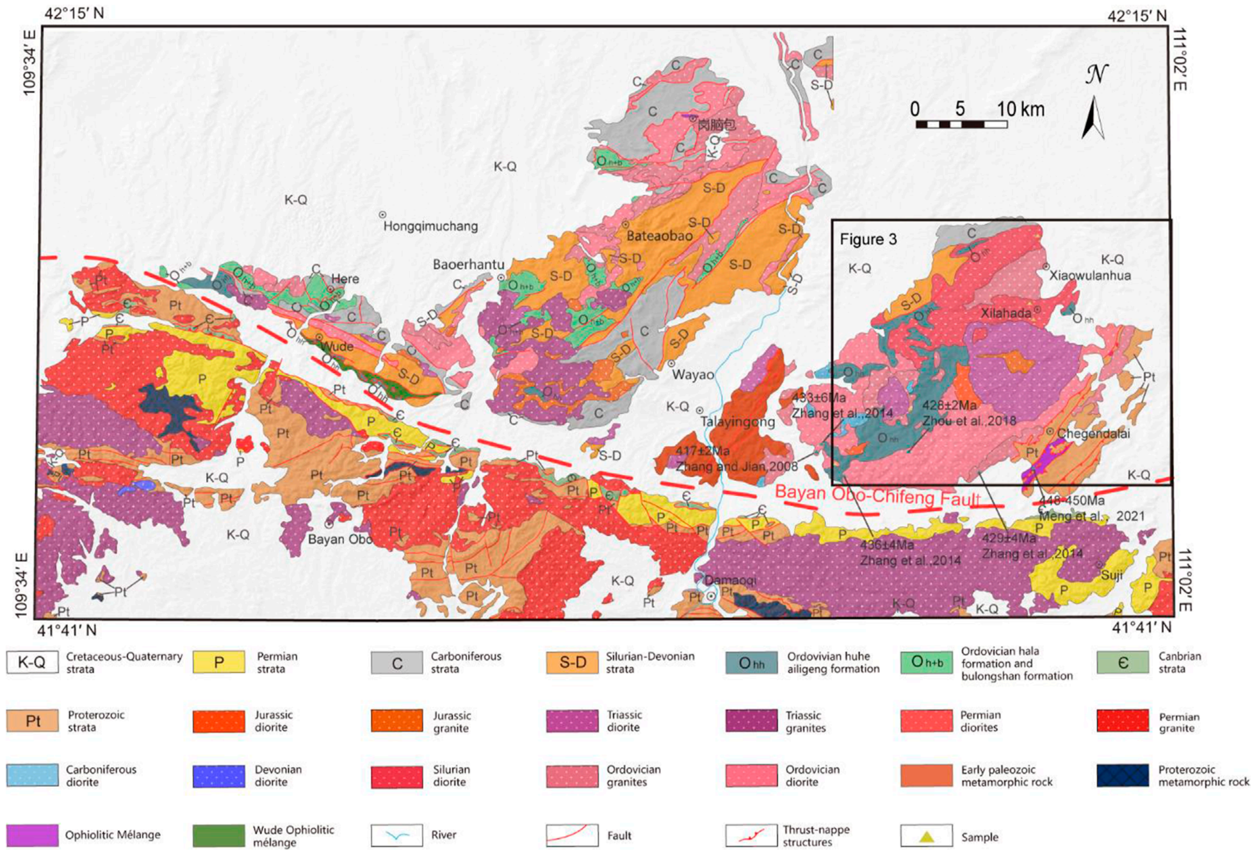

FIGURE 2
Geological map of the study area (modified after 1:25,000 Mandula and Bayan Obo sheets).

northern part of Damaoqi. It also aimed to elucidate the subduction mechanism and closure time of the South Bainaimiao Ocean in the Early Paleozoic.

2 Geological setting

The Xingmeng Orogenic Belt is located in the southeastern part of the Central Asian Orogenic Belt, within Chinese territory, which is subdivided from north to south into the Uliastai continental margin, Hegenshan ophiolitic mélanges, the Northern Orogenic Belt, the Solonker Suture Zone, and the Southern Orogenic Belt (Figure 1B). The Southern Orogenic Belt comprises, from north to south, the Ondor Sum subduction accretion complex and the Bainaimiao arc (Xiao et al., 2003; Zhang and Jian, 2008; Xu et al., 2013; Zhang et al., 2018; Yang et al., 2019).

The Ondor Sum subduction accretion complex extends southward to the Bainaimiao arc, bounded by the Xar Moron Fault (Figure 1B) (Xiao et al., 2003). The Early Paleozoic Ondor Sum subduction accretion complex, formed by the southward subduction of the Paleo-Asian Ocean, consists primarily of greenschists, carbonate lens bodies, muscovite-quartz schists, quartzites, and interbedded marble layers. This subduction accretion complex is overlain unconformably by Carboniferous and Permian volcanic and sedimentary rocks (Zhou et al., 2018). Scholars have reported mylonite ages indicating subduction-related high-pressure metamorphic events at 453–449 Ma and subduction-type ophiolites at 490–450 Ma in this area (Jong et al., 2006; Xiao et al., 2015; Xu et al., 2013; Zhang and Jian, 2008).

The Bainaimiao arc is situated between the Ondor Sum subduction accretion complex and the North China Craton (NCC), delineated by the Bayan Obo-Chifeng fault (Figure 1B) (Xiao et al., 2003). The Bainaimiao arc displays abundant Early Paleozoic intrusive rocks including tonalite, quartz diorite, granodiorite, and granite, indicative of subduction or collision-related settings. It also features magmatic rocks such as basalt and andesite (Zhang and Jian, 2008; Liu et al., 2013; Zhang et al., 2013; Zhang et al., 2014; Zhou et al., 2018; Chen et al., 2020; Hu et al., 2022; Li et al., 2023). Zircon U-Pb dating of dacite in the western segment of the Bainaimiao arc yields an age of 447 Ma (Hu et al., 2022). SHRIMP zircon U-Pb dating indicates intrusion ages of 452 ± 3 Ma, 446 ± 2 Ma, and 440 ± 2 Ma for gabbro, quartz diorite, and granodiorite respectively in the Damaoqi area. The age of 417 ± 2 Ma for tonalite is interpreted as magmatic activity related to arc-continent collision at the northern margin of the NCC (Zhang and Jian, 2008). Zircon U-Pb ages and geochemical characteristics indicate that activity in the Bainaimiao arc spanned from 520 to 420 million years ago (Zhang et al., 2014). Gabbro ages of 453–431 Ma, granite ages of 441–436 Ma, and sedimentary rock ages of 441 Ma have been reported in this area (Chen et al., 2020). Hence, the Early

Paleozoic magmatic rocks of the Bainaimiao arc are predominantly concentrated in the Ordovician to Silurian periods. The Middle-Late Silurian Xuniwusu Formation and the Late Silurian-Early Devonian Xibiehe Formation unconformably overlie the island arc magmatic rocks. The Xuniwusu Formation comprises Middle-Late Silurian turbidite sediments predominantly composed of sandstone, siltstone, and mudstone. The Xibiehe Formation, on the other hand, consists of Late Silurian-Early Devonian molasse sediments, interpreted as products of arc-continent collision termination (Zhang and Jian, 2008; Zhang et al., 2014).

Between the Bainaimiao arc and the NCC lie the Wude ophiolitic mélange belt and the Chegenda ophiolitic mélange belt (Figure 2). The Wude ophiolitic mélange belt comprises ultrabasic rocks, gabbro, and Ordovician arc-related magmatic rocks (Jia et al., 2003; Zhang et al., 2014). However, the controversy surrounding this Ordovician ophiolitic mélange belt is beyond the scope of this paper. The Chegenda ophiolitic mélange includes Ordovician-Silurian gabbro, basalt, peridotite, diabase, and schist (Zhang et al., 2014; Meng et al., 2021). Both the Wude and Chegenda ophiolitic mélange belts have been intruded by Late Paleozoic granitic plutons and overlain by Late Paleozoic to Cenozoic strata.

The northern margin of the North China Craton comprises a Precambrian crystalline basement and sedimentary cover ranging from the Paleozoic to Mesozoic Eras. The basement primarily comprises Archean to Paleoproterozoic magmatic and metamorphic rocks. Over the Precambrian basement, the sequence comprises the Mesoproterozoic to Neoproterozoic (~1600-850 Ma) Bayan Obo Group and Late Paleozoic magmatic rocks (Zhang et al., 2017; Zhou et al., 2018a). Late Paleozoic magmatic rocks primarily occur in the Carboniferous and Permian periods and include rhyolite, andesite, and volcanic breccia. (Tang et al., 2021).

The Chegendalai ophiolitic mélange belt extends approximately 15 km predominantly southeastward. Its margins display well-developed fractures, contacting the overlying Mesoproterozoic Baiyinbaolage Formation quartzite and muscovite quartz schist along fault planes oriented at 160° strike and 35° dip. The mélange comprises both blocks and a matrix. The blocks vary in size and mainly consist of peridotite, pyroxenite, gabbro, basalt, and limestone. The matrix is predominantly schist, and both blocks and matrix display faulted structural contacts (Figures 3, 4).

Ultrabasic rock blocks in the mélange zone are extensively fractured by tectonic activity. Weathered surfaces are gray-white to gray-black, with fresh surfaces showing a light yellow-green color often in lens-shaped forms (Figures 5A, C, E). Gabbro blocks in the mélange zone are predominantly lens-shaped. Some gabbro blocks have undergone late-stage regional metamorphism and ductile shear deformation, forming mylonitized gabbro (Figure 5D). The gabbro rock is gray-green, with zoisite being the predominant alteration mineral. Diabase porphyrite in the mélange zone occurs in blocky and lens-shaped forms, undergoing weaker structural deformation and metamorphism compared to ultrabasic rocks and gabbros, and is in structural contact with surrounding rocks. The rock shows a weathered surface in grayish-green, with the fresh surface appearing light grayish-green, displaying a diabasic porphyritic texture. Internally, there is slight chloritization and actinolitization (Figure 5B). The plagioclase actinolite schist matrix is in fault contact with rock blocks, with the exposed weathered surface appearing gray-black, and the fresh surface gray-black to gray-green. The rock is relatively fragmented with well-developed foliation (Figures 5A, C).

The Arigong and Xilahada areas in the northern part of Chegendalai are characterized by extensive distribution of arc magmatic rocks, consisting mainly of quartz diorite, tonalite, and granodiorite (Figure 3). Quartz diorite has a weathered surface that is gray-black, with its fresh surface appearing gray-green, displaying a blotchy structure and blocky texture (Figures 6A, B). Granodiorite has a weathered surface that is gray-white to gray-black, with its fresh surface appearing gray-white, displaying a medium to fine-grained granitic structure with a blocky texture (Figures 6C–E, G). Tonalite has a weathered surface that is gray-black, with its fresh surface appearing gray-white, showing a medium to fine-grained granitic structure with a blocky texture. In the field, occurrences of granodiorite intruded by tonalite are observed (Figure 6F).

3 Sampling and methods

A total of 37 samples were collected for this study, with their locations illustrated in (Figures 3, 4). These samples include nine ultrabasic rock samples (DME_5-TW_1, DME_5-$YQ_{1\text{-}5}$, DME_7-$YQ_{1\text{-}3}$), two gabbro samples (DME_6-$YQ_{1\text{-}2}$), and one diabase porphyrite sample (DMX). One schist sample was collected, specifically plagioclase actinolite schist (DME_{10}-TW_1). A total of 24 samples of intermediate-acid magmatic rocks were collected, consisting of tonalite ($XLHD_1$-TW_1, XLHD1-$YQ_{1\text{-}3}$), quartz diorite (ARG_2-$YQ_{1\text{-}3}$, ARG_4-$YQ_{1\text{-}3}$), and granodiorite ($XLHD_2$-TW_1, $XLHD_2$-$YQ_{1\text{-}3}$, $XHDT_1$-TW_1, $XHDT_1$-$YQ_{1\text{-}3}$, $TLMM_1$-$YQ_{1\text{-}3}$, $XWLH_1$-$YQ_{1\text{-}3}$). Sample Form Supplementary Table S1.

The OLYMPUS-BX53 detection equipment was used under environmental conditions of 21°C–25°C temperature and 50%–70% relative humidity. The selected zircon samples were sent to Beijing Zhongke Mining Research and Testing Technology Co., Ltd. Zircon grains intended for analysis were mounted in resin and imaged using scanning electron microscopy for cathodoluminescence (Figure 9). The zircon selection, target fabrication, and cathodoluminescence imaging of the diabase porphyrite (DMX) samples were conducted at the Beijing National Geological Testing Center (Figure 9F). Zircon targets were sent to the Institute of Geomechanics, Chinese Academy of Geological Sciences for LA-ICP-MS zircon U-Pb dating analysis. The analysis was conducted using the GeoLas Hd 193 nm ArF excimer laser ablation system and an Agilent 7,900 quadrupole inductively coupled plasma mass spectrometer at the Key Laboratory of Paleomagnetism and Paleotectonic Reconstruction, Ministry of Natural Resources. Standard zircon 91,500, with a spot size of 32 μm, was used as the external standard (Wang et al., 2022). Zircon U-Pb isotope dating of diabase porphyrite samples was conducted using LA-ICP-MS at the North China Mineral Resources Supervision and Testing Center, Tianjin Institute of Geological Survey, China Geological Survey. Concordia diagrams and detrital zircon age frequency distribution plots were analyzed with Isoplot (Ludwig, 2003). Age distribution comparison histograms were created with DensityPlotter 7.2 (Vermeesch, 2012). Zircons older than 1,000 Ma were dated using ^{207}Pb-^{206}Pb ages, and those younger than 1,000 Ma were dated using ^{206}Pb-^{238}U ages.

Whole rock geochemical analysis samples undergo initial screening. Fresh, uncontaminated samples are then crushed to

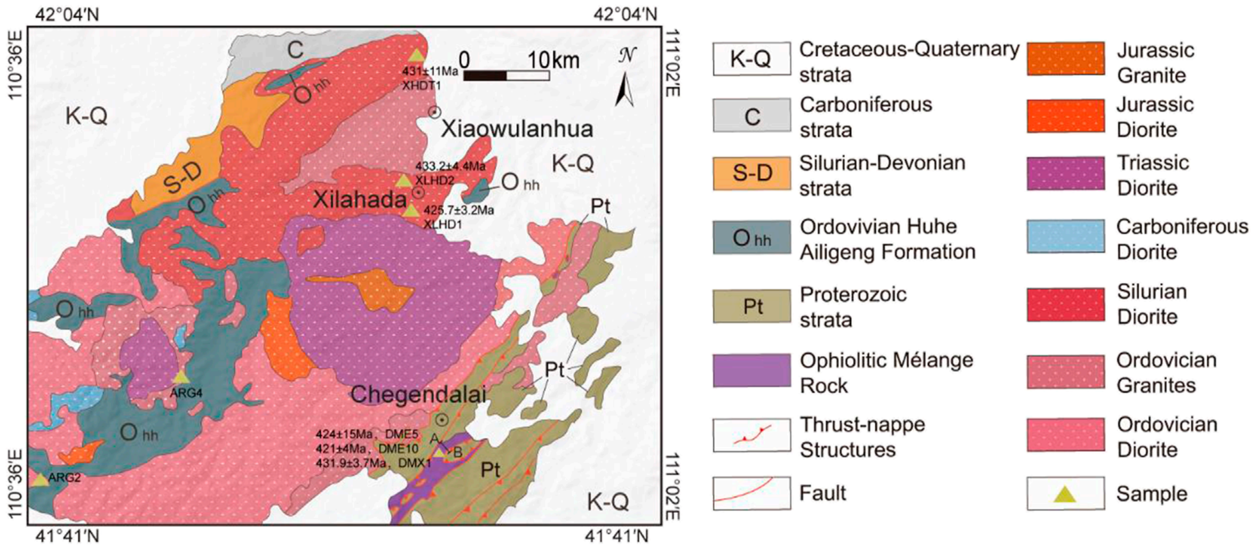

FIGURE 3
Simplified map of the study area and sampling locations.

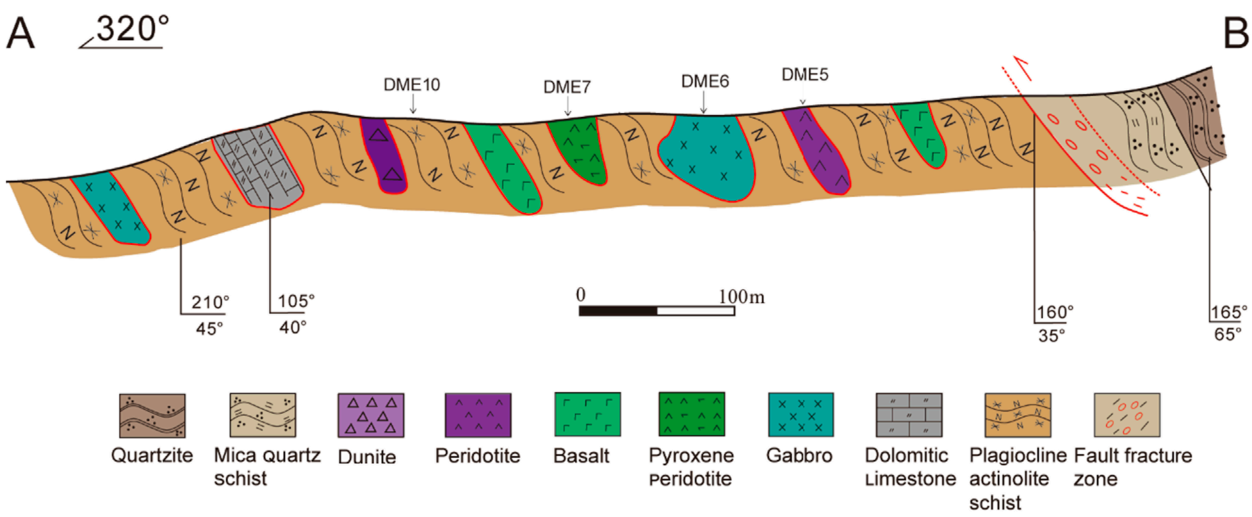

FIGURE 4
Profile of the Chegendalai ophiolitic mélange. The AB is the end point and the starting point of the profile, respectively, and the specific location is reflected in Figure 3.

200 mesh size at the Hebei Regional Geological Survey Institute laboratory before being sent to the Beijing National Geological Testing Center for analysis of major elements, trace elements, and rare earth elements content. Major elements were analyzed using X-ray fluorescence spectrometry (PW4400), following methods specified in national standard GB/T 14,506.28–2010. Trace elements and rare earth elements were analyzed using inductively coupled plasma mass spectrometry (PE300Q), following methods strictly adhering to national standard GB/T 14,506.30–2010. FeO, $H2O^+$, Cr, and LOI were tested according to national standards GB/T 14,506.14–2010, GB/T 14,506.2–2010, Q/GD 001–2002, and GB/T 14,506.34–2019, respectively.

4 Results

4.1 Petrography

The ultrabasic rocks within the mélange belt exhibit metasomatic structures and have undergone extensive serpentinization. Most minerals in these rocks have transformed into fibrous serpentine, with no residual minerals remaining (Figures 7A, B, D).

Most of the gabbro rocks have altered to zoisite. Locally, some original features persist, including plate-like plagioclase and granular pyroxene, which are indicative of a typical gabbro structure. Microscopic examination reveals that the gabbro consists

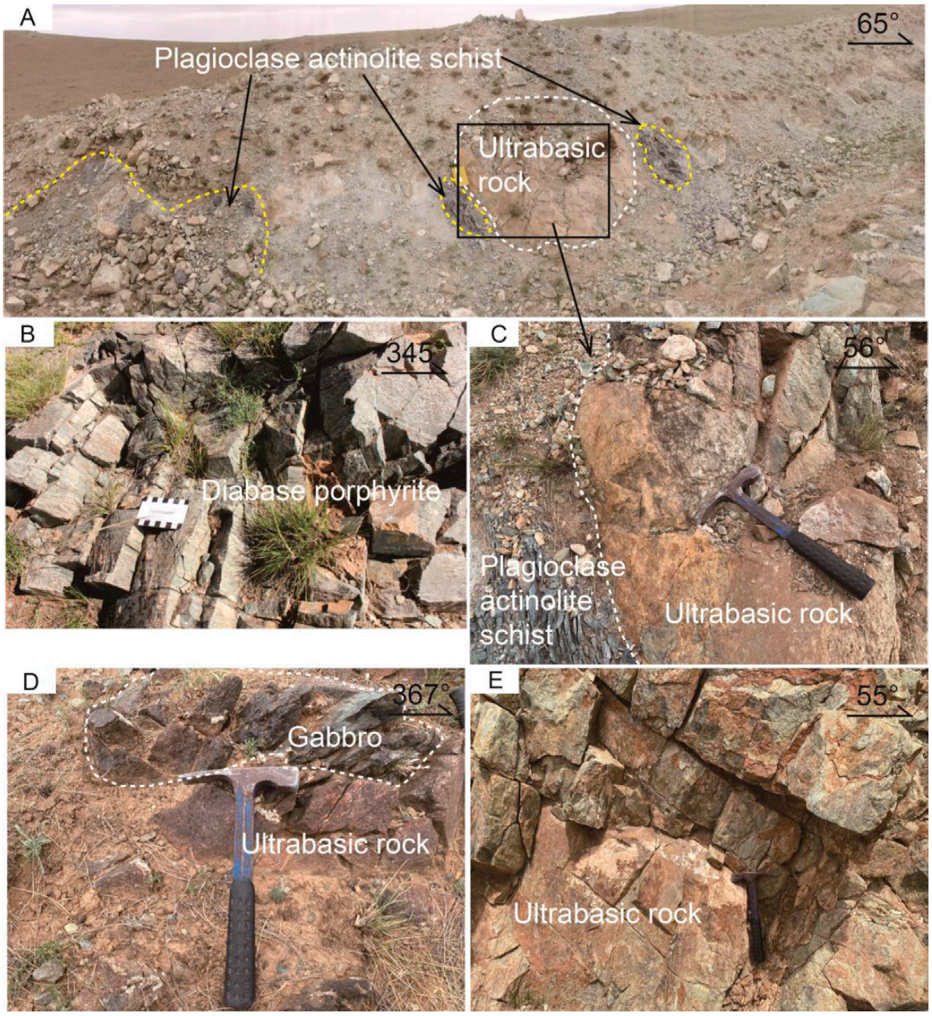

FIGURE 5
Sampling points for ultrabasic rocks **(A, C, E)**, gabbros **(D)**, plagioclase actinolite schist **(A, C)** and diabase porphyrite **(B)**.

predominantly of actinolite (60%) and analcime (37%–40%), with minor albite present. No residual crystals are preserved elsewhere (Figure 7C).

The diabase porphyrite shows slight chloritization and actinolization. Porphyroblasts in the rock mainly consist of granular and columnar hornblende (5%). The matrix is predominantly composed of granular plagioclase (45%), columnar pyroxene (35%), and a small amount of granular hornblende (10%) (Figure 7F).

The plagioclase amphibole schist consists of light green columnar actinolite (40%) arranged in a banded top-line pattern, forming a sheet-like structure. Interspersed among these minerals are granular quartz (20%) and plagioclase (35%), forming a lenticular and banded structure between the columnar actinolites. Some plagioclase grains exhibit slight sericitization and actinolization. Additionally, a small amount of biotite (5%) occurs in flake and scaly orientations (Figure 7E).

The quartz diorite exhibits a porphyritic and massive structure. It consists of plagioclase (45%), hornblende (30%), quartz (15%), and a small amount of biotite (10%). The minerals are irregularly distributed. The plagioclase shows sericitization, while the amphibole locally contains tin-bearing minerals and has been metasomatized by biotite schistosity (Figure 8A).

The granodiorite exhibits a medium to fine-grained granite structure with a massive appearance. The rock consists primarily of plagioclase (40%–55%), quartz (25%), potassium feldspar (10%–25%), with minor amounts of biotite and muscovite (10%–15%), exhibiting irregular mineral distribution. The plagioclase grains exhibit zirconization and contain biotite along with minor metasomatic plagioclase. Biotite and muscovite occur as scattered flakes, with some biotite showing chloritization and muscovitization (Figures 8B, D–F).

The tonalite exhibits a medium to fine-grained granite structure with a blocky appearance. The rock is primarily composed of plagioclase (65%), quartz (20%–25%), and biotite (10%–15%), with minerals irregularly distributed. Some plagioclase exhibits potassium feldspar, and flake biotite ranges in color from light yellowish brown to brown (Figure 8C).

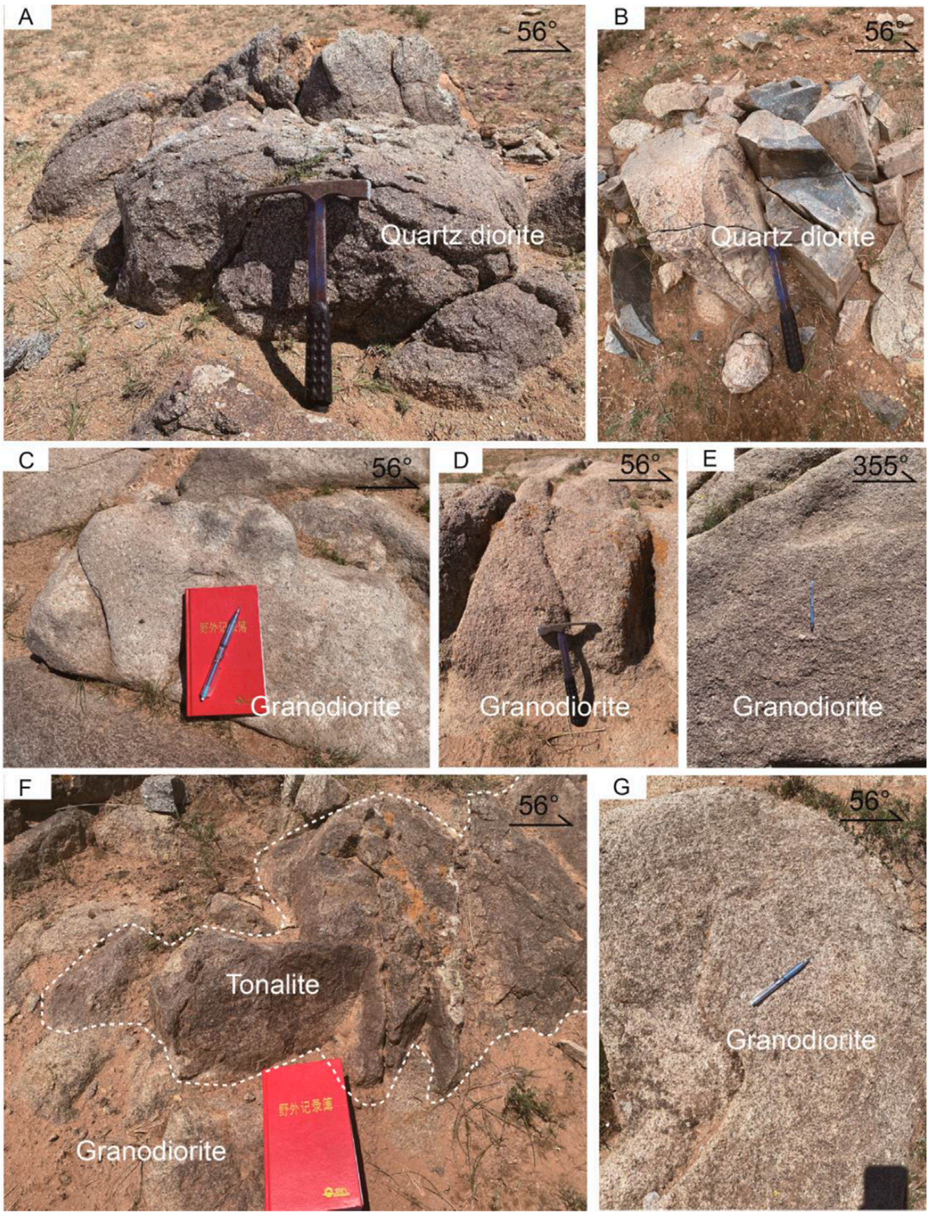

FIGURE 6
Sampling points of quartz diorite **(A, B)**, tonalite **(F)**, and granodiorite **(C–E, G)**.

4.2 Zircon U-Pb dating

This study conducted age dating on ultrabasic rocks (DME_5-TW_1), plagioclase actinolite schist (DME_{10}-TW_1), and island arc intermediate-acid magmatic rocks ($XHDT_1$-TW_1, $XLHD_1$-TW_1, $XLHD_2$-TW_1). The LA-ICP-MS zircon U-Pb dating results are presented in Supplementary Tables S2, S3.

Twenty-seven zircon grains were selected for dating from the ultrabasic rock sample DME_5-TW_1. The zircons are mainly tabular, with some being granular, having grain sizes ranging approximately from 40 to 100 μm, and generally exhibiting poor crystal shapes. Zircon exhibits oscillatory zoning, with Th/U ratios ranging from 0.05 to 2.5, averaging 0.65, indicative of a magmatic origin (Figure 9A). Twenty data points with high concordance were selected to construct a concordia diagram. The weighted mean age of four zircons using ^{206}Pb-^{238}U dating is 424 ± 15 Ma (MSWD = 4.5) (Figure 10A). The older zircon age may represent the inherited zircon age. The rock was modified by the late Permian magma and mixed with young zircons (Zhang et al., 2014).

One hundred detrital zircon grains were selected for dating from the Plagioclase actinolite schist sample DME_{10}-TW_1. The zircon grains have diameters ranging approximately from 20 to 130 μm, exhibit clear oscillatory zoning, and have Th/U ratios ranging from 0.08 to 3.26 with an average of 0.71, typical of magmatic zircons, and are relatively fractured (Figure 9B). Ninety-seven zircon grains with relatively high concordance were selected to construct a concordia

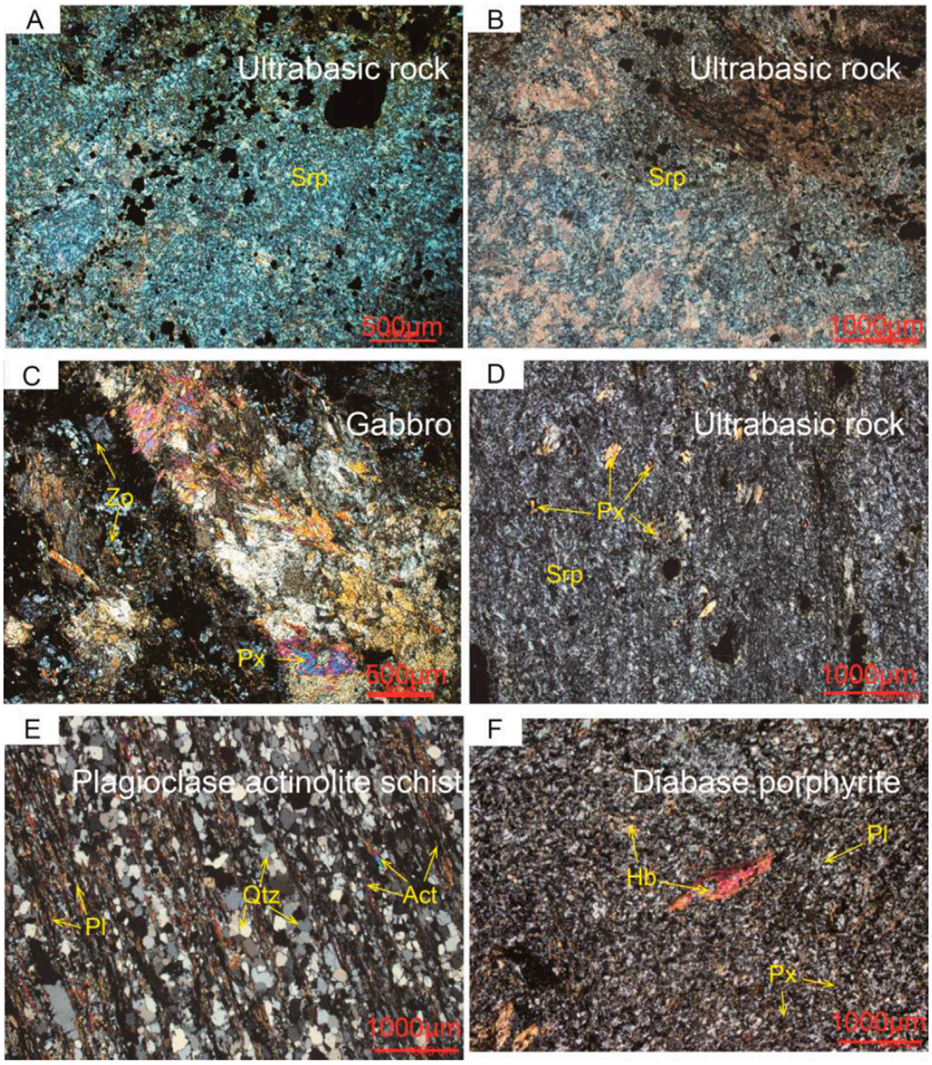

FIGURE 7
Under the microscope characteristics of ultrabasic rock **(A, B, D)**, gabbros **(C)**, diabase porphyrite **(F)**, and Plagioclase actinolite schist **(E)** samples (Qtz, quartz; Pl, plagioclase; Srp, serpentine; Px, pyroxene; Act, actinolite; Hb, hornblende; Zo, zoisite).

diagram and detrital zircon age spectrum. The detrital zircons show predominant age peaks at 430 Ma and 1800 Ma (Figure 11). After excluding younger zircon ages influenced by later events (273 ± 4 Ma and 395 ± 3 Ma), the remaining young detrital zircon ages concentrate around 432.9 ± 3.5 Ma, with the youngest age being 421 ± 4 Ma, interpreted as the protolith age of the schist (Figure 10F).

Thirty zircon grains were selected for dating from the diabase porphyrite sample DMX_1-TW_1. The zircon grains have diameters ranging from 50 to 120 μm, with a length-to-width ratio generally around 1:1 or 2:1. Most zircon grains exhibit clear oscillatory zoning, and Th/U ratios are concentrated between 0.41 and 0.99, displaying typical characteristics of magmatic zircons (Figure 9F). Six zircon grains with relatively clustered ages were used for weighted mean age calculation, resulting in an age of 431.9 ± 3.7 Ma (MSWD = 0.87) (Figure 10E). This is interpreted as the crystallization age of the diabase porphyrite. The older zircon grains likely represent inherited zircons captured during diagenesis.

Zircon dating was conducted on twenty-five grains each from the diorite samples $XHDT_1$-TW_1, $XLHD_1$-TW_1, and $XLHD_2$-TW_1. The zircon grains in the samples are relatively large, approximately 100–240 μm in size, mostly elongated and short prismatic shapes. The Th/U ratios average 0.53, 0.32, and 0.47 respectively, with clear growth zoning, displaying typical characteristics of magmatic zircons (Figures 9C–E). The age data of 25 zircons measured by tonalite samples $XLHD_1$-TW_1 are relatively concentrated. The weighted average age of ^{206}Pb-^{238}U is 425.7 ± 3.2 Ma (MSWD = 3.1) (Figure 10B). In the granodiorite sample $XLHD_2$-TW_1, after excluding seven zircon grains with low concordance, a weighted mean ^{206}Pb-^{238}U age of 433.2 ± 4.4 Ma was obtained from the remaining 18 zircon grains (MSWD = 2.6) (Figure 10C). In the granodiorite samples $XHDT_1$-TW_1, the dating results have a low degree of concordance, with only six data points showing high concordance and reliability. Four concentrated ^{206}Pb-^{238}U ages are used for weighted average

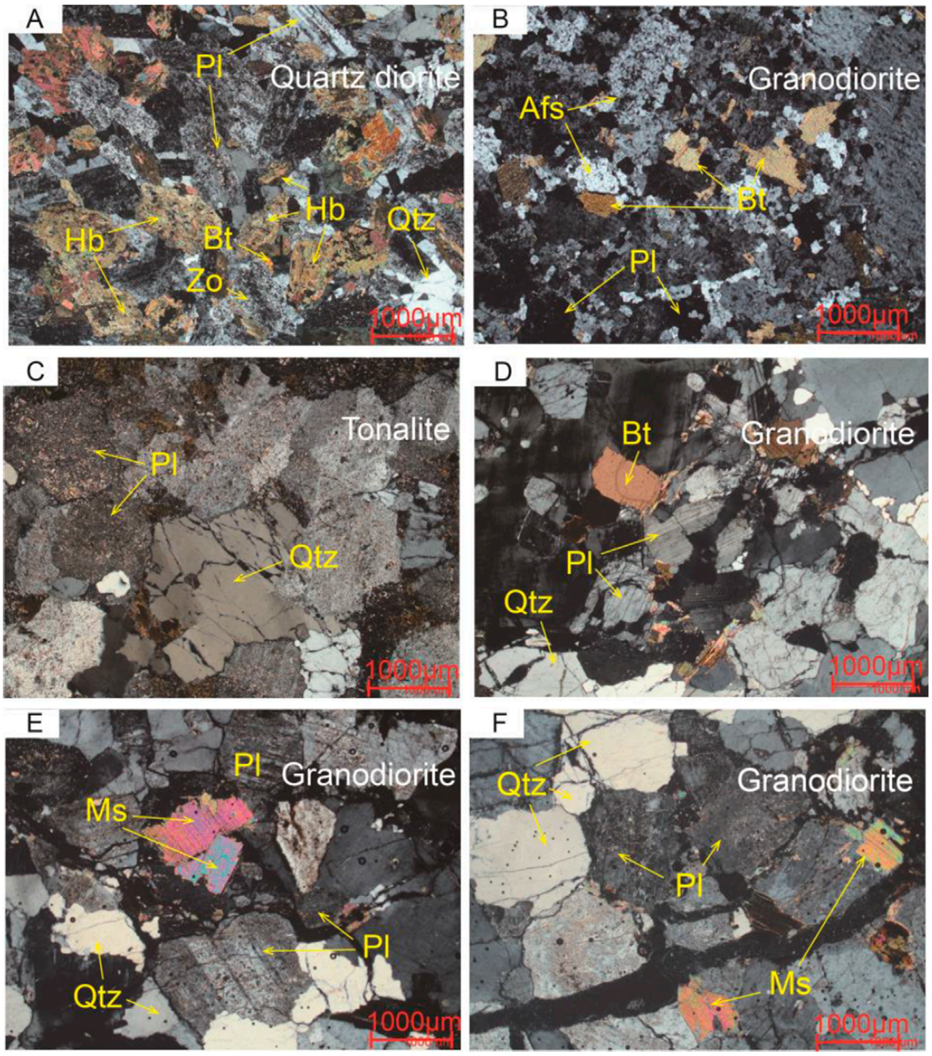

FIGURE 8
Microscopic features of intermediate to acidic magmatic rocks: Quartze diorite **(A)**, Granodiorite **(B, D–F)**and Tonalite **(C)** (Qtz, quartz; Pl, plagioclase; Ms, muscovite; Bt, biotite; Hb, hornblende; Afs, alkali feldspar).

calculation. The crystallization age of the magma is 431 ± 11 Ma (MSWD = 3.9) (Figure 10D).

4.3 Whole-rock geochemistry

4.3.1 Major elements

Supplementary Table S4 presents the results of major and trace element analyses for 28 samples.

Ultrabasic rocks have very low levels of K_2O (0.01 wt%), Na_2O (<0.01 wt%), and P_2O_5 (<0.01 wt%); relatively low levels of SiO_2 (38.96–41.69 wt%), Al_2O_3 (0.57–1.42 wt%), and CaO (0.09–4.18 wt%); low levels of TiO_2 (0.02–0.04 wt%) and MnO (0.07–0.14 wt%); and high levels of TFe_2O_3 (6.49–8.5 wt%), FeO (3.14–3.72 wt%), and MgO (33.04–35.31 wt%). Before mapping, loss on ignition is eliminated, and the rock's major elements are recalculated on a dry basis. In Figure 12A, ultrabasic rocks are concentrated mainly in the Olivine gabbro field, and they are shown as part of the tholeiitic series in Figure 12B.

Gabbros have relatively low levels of SiO_2 (43.77–45.98 wt%), K_2O (0.15–0.28 wt%), TiO_2 (0.51–0.63 wt%), and P_2O_5 (0.01 wt%); and high levels of CaO (12.38–16.89 wt%), MgO (8.65–9.21 wt%), Al_2O_3 (15.28–18.32 wt%), TFe_2O_3 (8.8–12 wt%), and FeO (4.98–8.86 wt%). Before mapping, loss on ignition is eliminated, and the rock's major elements are recalculated on a dry basis. In Figure 12A, gabbros are concentrated mainly in the Olivine gabbro field, and they are shown as part of the tholeiitic series in Figure 12B.

Diorites have low levels of TFe_2O_3 (2.68–3.05 wt%), P_2O_5 (0.13–0.14 wt%), TiO_2 (0.09–0.36 wt%), and MgO (1.11–1.26 wt%); and high levels of SiO_2 (64.5–65.53 wt%), Al_2O_3 (18.29–18.43 wt%), K_2O (2.73–3.46 wt%), and Na_2O (4.77–5.25 wt%). Granodiorites exhibit high levels of SiO_2 (66.77–74.01 wt%), Al_2O_3 (14.35–17.49 wt%), K_2O (1.88–4.63 wt%), and Na_2O (3.35–4.83 wt%); and low levels of TFe_2O_3 (0.99–2.79 wt%), P_2O_5 (0.02–0.11 wt%), TiO_2

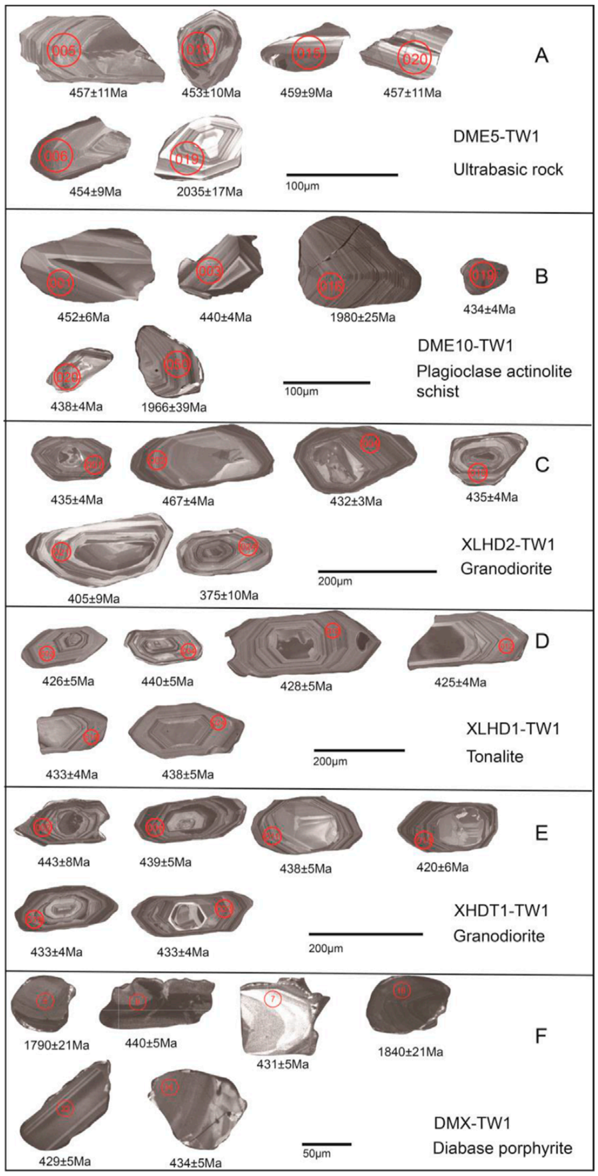

FIGURE 9
Cathodoluminescence (CL) image of representative zircons: ultrabasic rock **(A)**, Plagioclase actinolite schist **(B)**, Granodiorite **(C, E)**, Tonalite **(D)** and diabase porphyrite **(F)**.

(0.09–0.36 wt%), and MgO (0.28–1.01 wt%). Quartz diorites exhibit high levels of SiO_2 (58.36–73.78 wt%), Al_2O_3 (14.49–16.5 wt%), K_2O (1.96–4.12 wt%), and Na_2O (3.71–4.3 wt%); and low levels of TFe_2O_3 (0.88–5.8 wt%), P_2O_5 (0.05–0.2 wt%), TiO_2 (0.02–0.6 wt%), and MgO (0.09–4.75 wt%). Before mapping, loss on ignition is eliminated, and the rock's major elements are recalculated on a dry basis. In Figure 12A, intermediate-acid magmatic rocks are primarily concentrated in the diorite-granite region, depicted as part of the calc-alkaline series in Figure 12B.

4.3.2 Trace elements

The chondrite-normalized rare earth element spidergrams of gabbroic nodules exhibit low total rare earth element content, depleted LREEs, flat HREEs, resembling E-MORB characteristics, and significant positive Eu anomalies (δEu=1.30–2.46) (Figure 13C). The primitive mantle-normalized spidergrams show enrichment of LILEs (e.g., Rb, Ba, K, Pb, Sr) and significant depletion of HFSEs (e.g., Nb, Zr, Hf) (Figure 13D).

The chondrite-normalized rare earth element spidergrams of ultrabasic rock show a slightly low total rare earth element content, with a slight trend of LREE enrichment and HREE depletion to slight enrichment, and positive (δEu=1.03–1.99) or negative (δEu=0.62–0.69) Eu anomalies (Figure 13C). The primitive mantle-normalized spidergrams show enrichment of LILEs (e.g., U, Pb, Sr) and depletion of HFSEs (e.g., Nb, Zr, Hf) (Figure 13D).

The chondrite-normalized rare earth element spidergrams of intermediate-acid magmatic rocks show enrichment of LREEs and depletion of HREEs. Quartz diorites exhibit a prominent negative Eu anomaly (δEu=0.56–0.93), while the other samples do not show significant Eu anomalies (Figure 13A). The primitive mantle-normalized spidergrams for most samples show lower contents of HFSEs (e.g., Nb, Ta, *p*, and Ti) and higher contents of LILEs (e.g., Ba, K, Pb, and Sr) (Figure 13B).

5 Discussion

5.1 Formation ages

Previous studies in the Chegendalai area dated gabbro blocks to be 448–450 Ma using LA-ICP-MS zircon U-Pb geochronology (Meng et al., 2021). This study indicates that the formation age of the rock mass in the ophiolite is Middle-Late Silurian (431.9–424 Ma). The ophiolite in the ophiolitic mélange zone thus represents the lower limit of oceanic crust existence around 424 Ma, indicating ocean closure occurred after 424 Ma. Therefore, the formation age of the ophiolite spans from Late Ordovician to Late Silurian (450–424 Ma), indicating the South Bainaimiao Ocean it represents existed from at least 450 Ma to around 424 Ma. The plagioclase actinolite schist age of the matrix in the Chegendalai ophiolitic mélange is 421 Ma, representing the mixing age of the ophiolitic mélange, indicating mixing occurred by the Late Silurian. The South Bainaimiao Ocean closed during the Late Silurian, just before 421 Ma. Ophiolite emplacement occurred within 10 million years after the formation of the oceanic lithosphere it represents (Smith and Rassios, 2003). In summary, the formation period of this ophiolite is Late Ordovician to Late Silurian. Emplacement occurred slightly after the youngest block age (424 Ma), and mixing occurred before 421 Ma, forming the ophiolitic mélange.

Previous studies extensively investigated the timing of formation of the Bainaimiao Island Arc Belt. Accurate SHRIMP zircon U-Pb ages from the Damaoqi area indicate intrusion ages of 452 ± 3 Ma for diorite, 446 ± 2 Ma for quartz diorite, and 440 ± 2 Ma for granodiorite (Zhang and Jian, 2008). The age of 417 ± 2 Ma for the tonalite indicates magmatic activity associated with the collision between the island arc and the northern margin of the NCC (Zhang and Jian, 2008). Combining regional zircon U-Pb ages and geochemical characteristics suggests that Bainaimiao arc activity occurred during the interval 0.52–0.42 Ga (Zhang et al.,

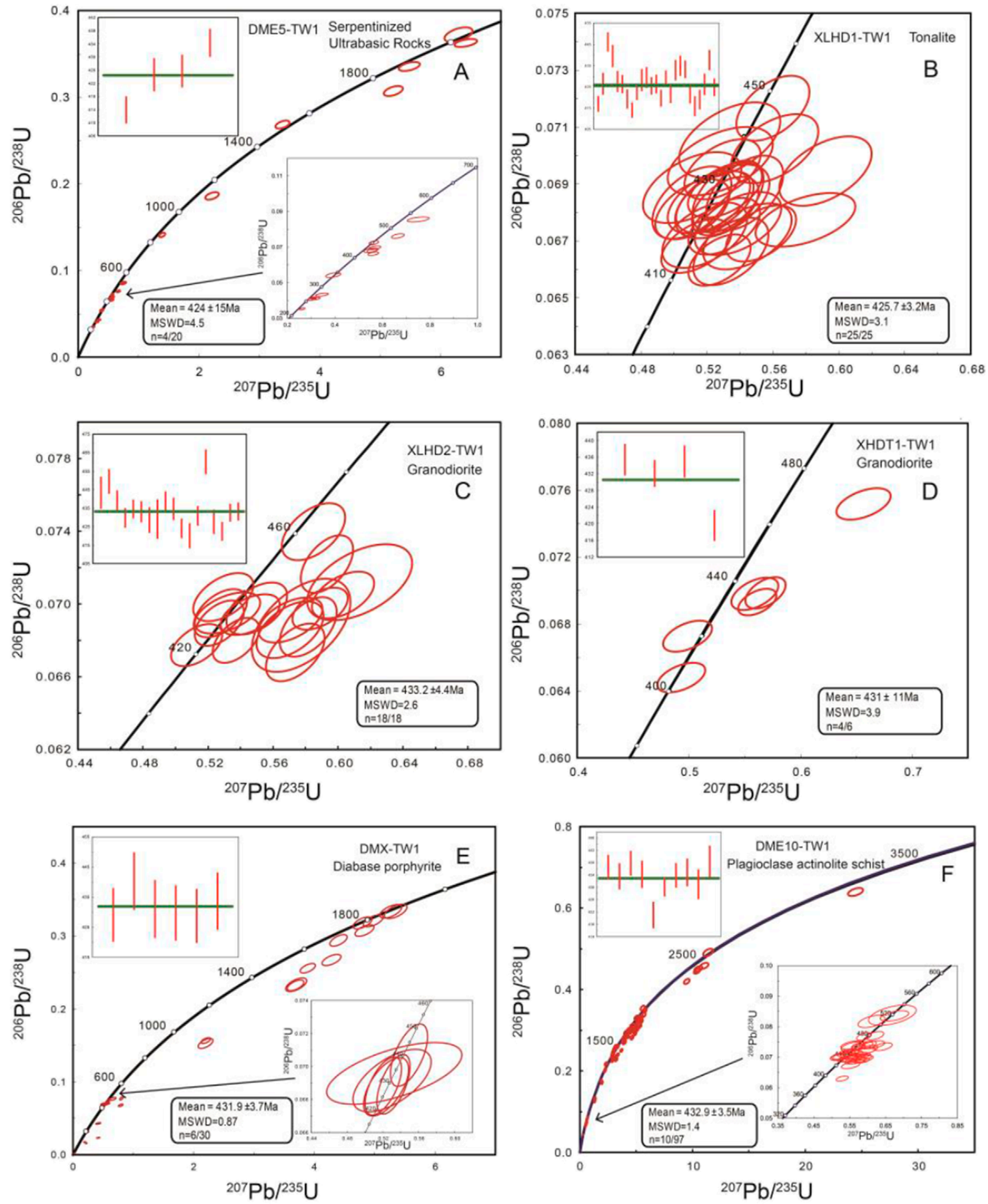

FIGURE 10
Concordia diagram and detrital zircon age spectrum: **(A)** Serpentinized ultrabasic rock, sample DME5-TW1; **(B)** Tonalite, sample XLHD1-TW1; **(C)** Granodiorite, sample XLHD2-TW1; **(D)** Granodiorite, sample XHDT1-TW1; **(E)** Diabase porphyrite, sample DMX1-TW1; **(F)** Plagioclase actinolite schist, sample DME10-TW1.

2014). Gabbro ages ranging from 453 to 431 Ma, granite ages from 441 to 436 Ma, and sedimentary rock ages of 441 Ma have all been reported in this region (Chen et al., 2020). Sedimentary ages of the Bainaimiao Group in the middle segment of the island arc belt range from 500 to 443 Ma (Gu et al., 2012; Liu et al., 2014; Zhang, J.F. et al., 2017; Zhang et al., 2020). In conclusion, the formation period of Bainaimiao Island arc magmatic rocks spans approximately from the Cambrian to the Silurian. The results of this study indicate zircon U-Pb ages of 425.7 Ma for the tonalite sample $XLHD_1$-TW_1, 431 Ma and 433.2 M for the granite diorite samples $XHDT_1$-TW_1 and $XLHD_2$-TW_1. Therefore, the formation period of the intermediate-acid magmatic rocks in the northern Damaoqi area is determined to be during the Middle Silurian.

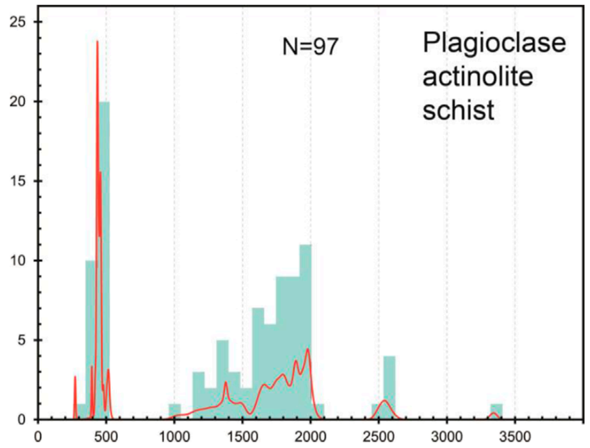

FIGURE 11
Detrital zircon age frequency distribution diagram of Plagioclase actinolite schist.

5.2 Genesis of magmatic rocks

In this study, the arc magmatic rocks and ophiolitic mélange exhibit geochemical similarities to the early Paleozoic magmatic rocks of the Bainaimiao arc. The ophiolitic mélange is predominantly found in the olivine diabase and sub-alkaline diabase ranges, while the arc magmatic rocks are concentrated in the intermediate to acidic diorite-granite ranges (Figure 12). The trace element characteristics of both the ophiolitic mélange and arc magmatic rocks align with the results of earlier studies from the Bainaimiao region (Figures 13, 14). Consequently, the island arc belt examined in this study represents the western extension of the Bainaimiao arc.

The Nb/La ratios ranging from 0.08 to 0.6 for gabbros and ultrabasic rocks indicate that the origin was from the lithospheric mantle (Smith et al., 1999). Geochemical signatures show that $(Th/Nb)_N > 1$ and $(Nb/La)_N < 1$ reliably indicate crustal contamination (Saunders et al., 1992; Kieffer et al., 2004). The $(Th/Nb)_N$ ratios range from 9.32 to 37.28 and $(Nb/La)_N$ ratios range from 0.07 to 0.58 for gabbros and ultrabasic rocks indicative of significant crustal assimilation. On the chondrite-normalized rare earth element spidergrams, gabbros have LREE depletion and slightly enriched HREEs. The distribution pattern is similar to N-MORB, and positive Eu anomalies ($\delta Eu = 1.30–2.46$), indicating plagioclase accumulation in the rock (Huang and Frey, 2003). Ultrabasic rocks have slight LREEs enrichment and slight HREEs depletion. The rare earth element distribution pattern is E-MORB and positive ($\delta Eu = 1.03–1.99$) or negative ($\delta Eu = 0.62–0.69$) Eu anomalies. On the primitive mantle-normalized spidergrams, gabbros are enriched in LILEs (e.g., Rb, Ba, K) and significantly depletion in HFSEs (e.g., Nb, Zr, Hf), indicating subduction-related characteristics (Pearce and Robinson, 2010; Ma et al., 2021). Ultrabasic rocks are enriched in LILEs (e.g., Sr, U, Pb) and depletion in HFSEs (e.g., Nb, Zr, Hf), indicating crustal characteristics (Hofmann, 1988). Therefore, gabbros and ultrabasic rocks likely originate from the lithospheric mantle of oceanic arcs or mid-ocean ridges and have undergone crustal assimilation.

Early Paleozoic magmatic rocks in the Bainaimiao island arc comprise diorite, tonalite, quartz diorite, and granodiorite compositions. Their geochemical characteristics indicate formation in an arc environment associated with subduction-related magmatism (Maniar and Piccoli, 1989; Barbarin, 1999; Zhang et al., 2014). Within the medium to acidic magmatic rocks, chondrite-normalized rare earth element spidergrams show enrichment of LREEs and depletion of HREEs, with most lacking significant Eu anomalies. The primitive mantle-normalized spidergrams reveal enrichment of LILEs (e.g., Rb, Ba, K, Pb) and depletion of HFSEs (e.g., Nb, Ta, Ti). The geochemical characteristics of the arc magmatic rocks and ophiolitic mélange display similarities, with identical element distribution patterns in the primitive mantle normalization diagrams (Figure 14). These trace element characteristics originate from fluids, melts, and supercritical fluids formed by dehydration melting of subducted slabs (Ma et al., 2019). Adakites are medium to acidic special island arc magmatic rocks composed of andesite, dacite, and rhyolite. The rocks are different with typical island arc magmatic rocks by lacking basalt and being characterized geochemically by high Sr, low Yb and Y contents, and a high Sr/Y ratio (Defant and Drummond, 1990; Martin, 1999). In this study, the northern Damaoqi medium-acidic island arc magmatic rocks exhibit high contents of Al_2O_3, Sr, Ba, and a high Sr/Y ratio, showing geochemical characteristics similar to adakites (Atherton and Petford, 1993; Stern and Kilian, 1996). Island arc magmatic rocks are positioned in the adakite field on $(La/Yb)_N$-Yb_N and Sr/Y-Y diagrams (Figure 15). Granodiorite, tonalite, and quartz diorite as early Paleozoic magmatic rocks in the Bainaimiao island arc may have formed due to partial melting of subducted slabs and interaction with the crust and mantle wedge (Xu et al., 2003; Tao et al., 2005).

On the Th/Yb-Ta/Yb diagram (Pearce, 1982) and the Th-Hf-Nb discrimination diagram (Wood, 1980), gabbro is situated within the VAB (Figure 16). On the Th/Yb-Ta/Yb diagram, ultrabasic rocks are situated within the WPB or MORB field. The Th-Hf-Nb discrimination diagram indicates the tectonic setting of VAB (Figure 16). On the Th/Yb-Ta/Yb discrimination diagram and the Th-Hf-Nb discrimination diagram, tonalite and quartz diorite situated in the VAB field (Figure 15). Granodiorite is classified as I-type granite in the Nb-SiO_2 and Zr-SiO_2 discrimination diagrams, and as VAG or syn-COLG in the Nb-Y diagram, and VAG in the Rb-(Yb+Ta) discrimination diagram (Figure 17). In summary, gabbro and ultrabasic rocks likely originate from the tectonic environments of volcanic arc basalt or mid-ocean ridges. The magmatic rocks in northern Damao Banner suggest a volcanic island arc setting.

5.3 Early paleozoic evolution of the south bainaimiao ocean

5.3.1 Subduction polarity

Recently, scholars have proposed the existence of the South Bainaimiao Ocean (Zhang et al., 2014), a viewpoint widely accepted by other researchers. However, considerable controversy exists regarding the subduction polarity of the South Bainaimiao Ocean (Zhang et al., 2014; Chen et al., 2020; Meng et al., 2021; Li et al., 2023; Zeng et al., 2023; Shi et al., 2024; Zhang et al., 2024). Previous studies indicate that during the early Paleozoic, the northern margin

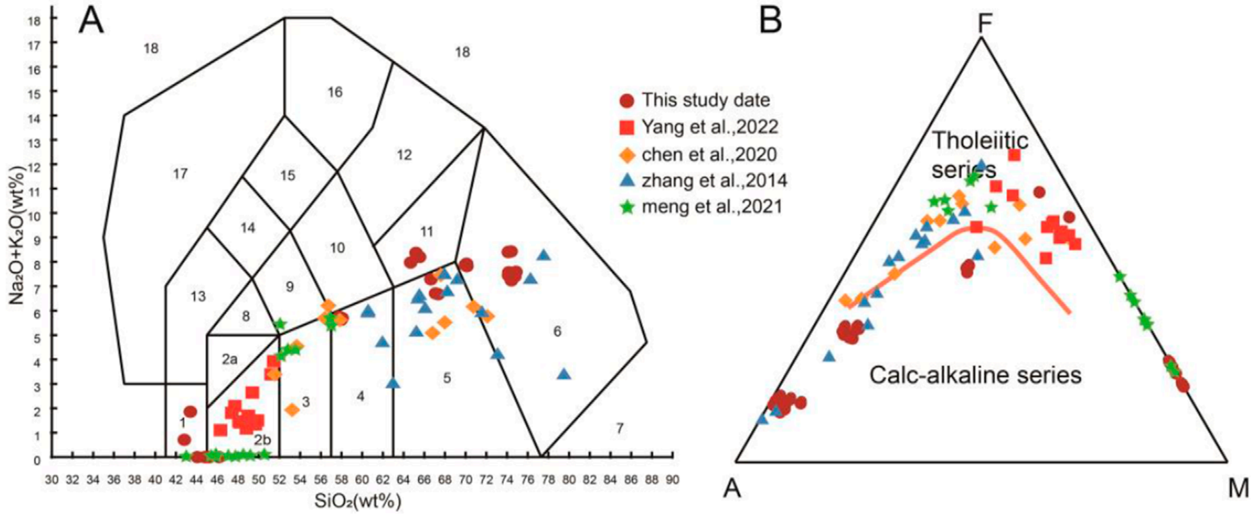

FIGURE 12
Geochemical classification diagrams: TAS diagram **(A)** (Middlemost, 1994) and AFM diagram **(B)** (Irvine and Baragar, 1971). 1 - Olivine gabbro; 2a - Alkaline gabbro; 2b - Subalkaline gabbro; 3 - Gabbro diorite; 4 - Diorite; 5 - Granodiorite; 6 - Granite; 7 - Silicon quartzite; 8 - Monzogabbro; 9 -Monzodiorite; 10 - Monzonite; 11 - Quartz Monzonite; 12 Syenite; 13 - Foid Gabbro; 14 - Foid Monzodiorite; 15 - Foid Monzosyenite; 16 - Foid Syenite; 17 -Foidolite; 18 - Sodalite/nepheline rock/pure leucite. Data for the early Paleozoic magmatic rocks from other locations of the Bainaimiao arc system are from Zhang et al. (2014), Chen et al. (2020), Meng et al. (2021), Hao et al. (2022).

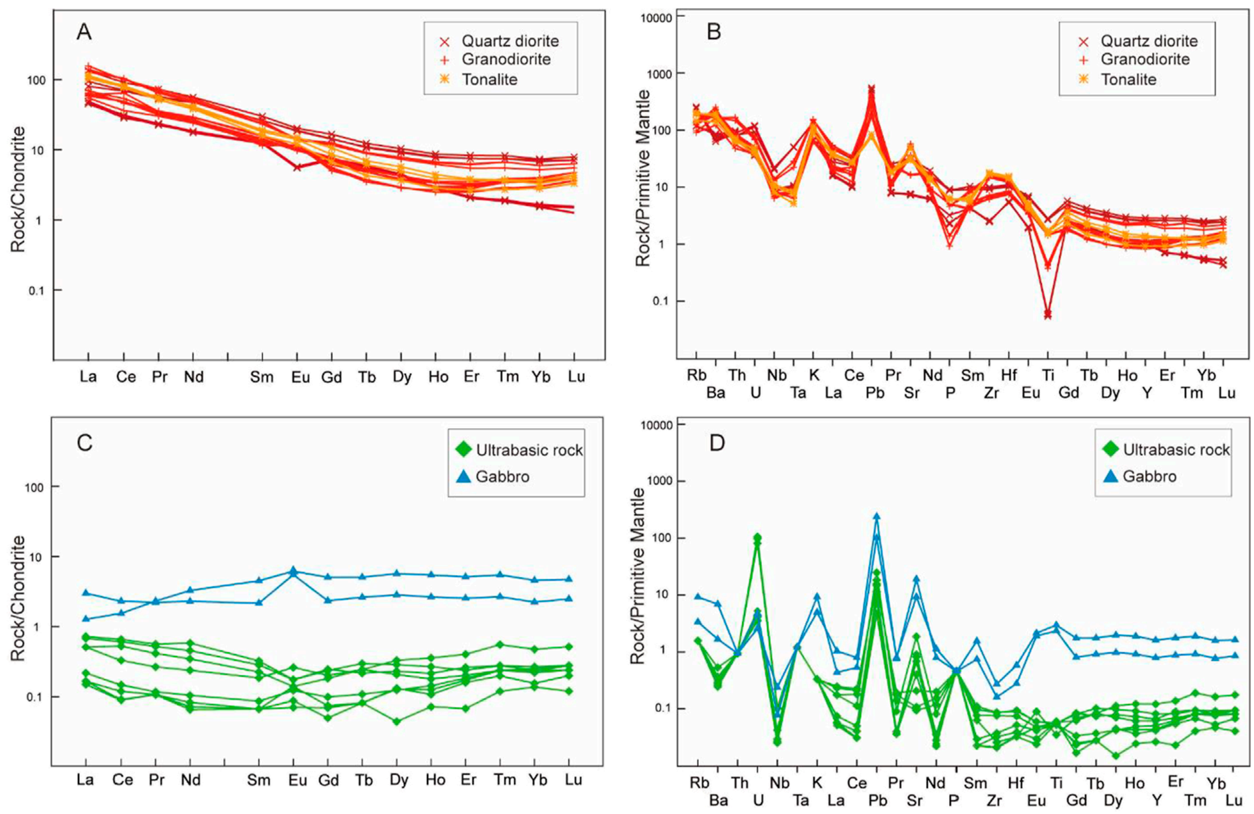

FIGURE 13
Chondrite-normalized rare earth element **(A, C)** and primitive mantle-normalized spidergrams **(B, D)**. Normalization data from Sun and McDonough (1989).

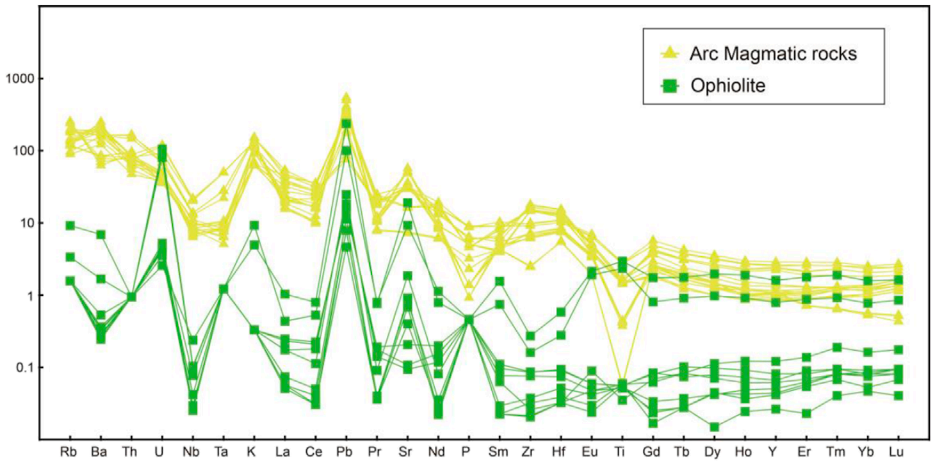

FIGURE 14
Primitive mantle-normalized spidergrams. Normalization data from Sun and McDonough (1989). Data for the early Paleozoic magmatic rocks from other locations of the Bainaimiao arc system are from Zhang et al. (2014), Chen et al. (2020), Meng et al. (2021), Hao et al. (2022).

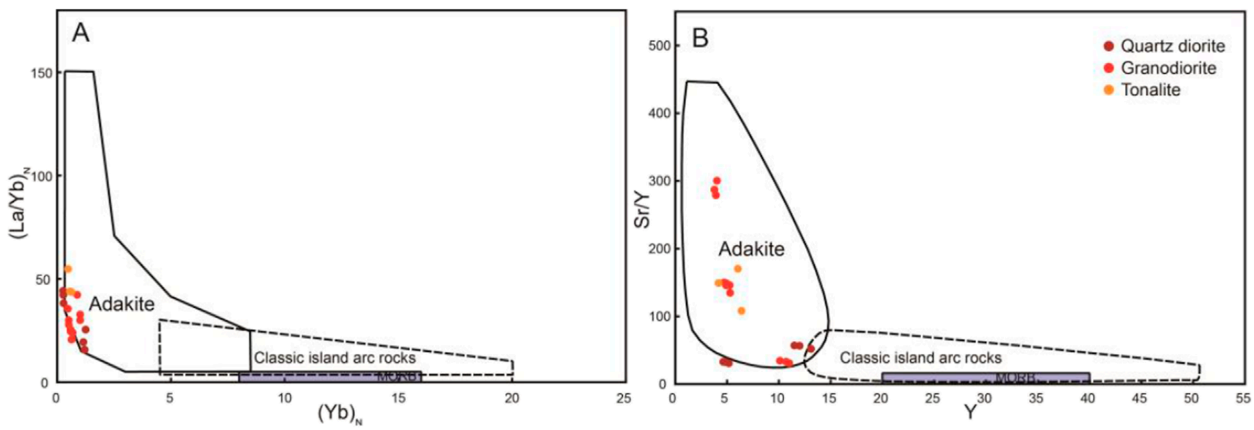

FIGURE 15
Discrimination diagrams for medium-acidic magmatic rocks in northern Damaoqi: **(A)** (La/Yb)N-YbN (Martin, 1986), and **(B)** Sr/Y-Y (Defant and Drummond, 1990; Drummond and Defant, 1990; Martin, 1999).

of the NCC was a passive continental margin (Xu and Chen, 1997; Li et al., 2009). Arc-related diorites and ultrabasic rocks have been reported in the Chegendalai serpentinite mélange (Meng et al., 2021). This study suggests that the Middle Silurian intrusive rocks in northern Damaoqi may have formed through partial melting of subducting plates interacting with mantle wedges, showing geochemical characteristics similar to adakites. Therefore, the South Bainaimiao Ocean should have subducted northward, with the NCC acting as a passive continental margin during this time.

5.3.2 Closure time of the south bainaimiao ocean

Previous studies have extensively investigated the timing of the South Bainaimiao Ocean closure. The tonalite in the Damaoqi area, dated at 417 Ma, is interpreted as a result of arc-continent collision subsequent to the closure of oceanic crust (Zhang and Jian, 2008). Scholars suggest the closure of the South Bainaimiao Ocean occurred around 420 Ma, based on the ages and geochemical characteristics of island-arc magmatic rocks in the Bayan Obo area (Zhang et al., 2014). Rhyolites from the southern part of the island arc, dated at 412 ± 1 Ma, exhibit Hf isotopic characteristics similar to those of the NCC (Qian et al., 2017). Middle to acidic rocks from the Late Silurian period and reverse thrust structures resulting from subduction collision in the Bainaimiao area indicate significant tectonic activity (Li et al., 2015; Zhou et al., 2018b). The development of quartz veins dated at 422.4 Ma further suggests a tectonic transition during mountain building in the Bainaimiao arc (Zhou et al., 2017). The unconformable overlay of the Late Silurian to early Devonian Xibiehe Formation over early Paleozoic ophiolites and arc-related magmatic rocks indicates the termination of the orogenic event (Zhang et al., 2004). During the Devonian period, the northern margin of the NCC developed a post-collisional extensional environment characterized by an alkaline rock belt (Shi et al., 2010; Zhang et al., 2010). Paleomagnetic data indicate that the southeastern part of the Central Asian Orogenic Belt amalgamated before the late Devonian period (Zhao et al., 2013). In this study, plagioclase actinolite schist as the matrix of ophiolitic

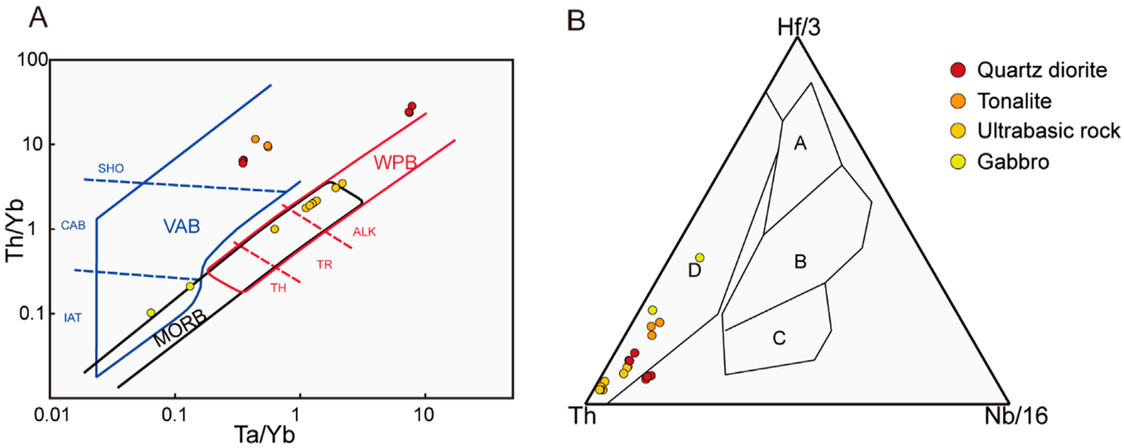

FIGURE 16
Tectonic discrimination diagrams: **(A)** Th/Yb-Ta/Yb diagram (Pearce, 1982): VAB - Volcanic Arc Basalt (IAT - Island Arc Tholeiite Basalt, CAB - Calc-Alkaline Basalt, SHO - shoshonitic), MORB - Mid-Ocean Ridge Tholeiite Basalt, WPB - Within Plate Basalt (TH - Tholeiitic, TR - Transitional, ALK - Alkaline); **(B)** Th-Hf-Nb diagram (Wood, 1980): A - N-type MORB, B - E-type MORB and Intraplate Tholeiite Basalt, C - Alkaline Intraplate Basalt, D - Volcanic Arc Basalt.

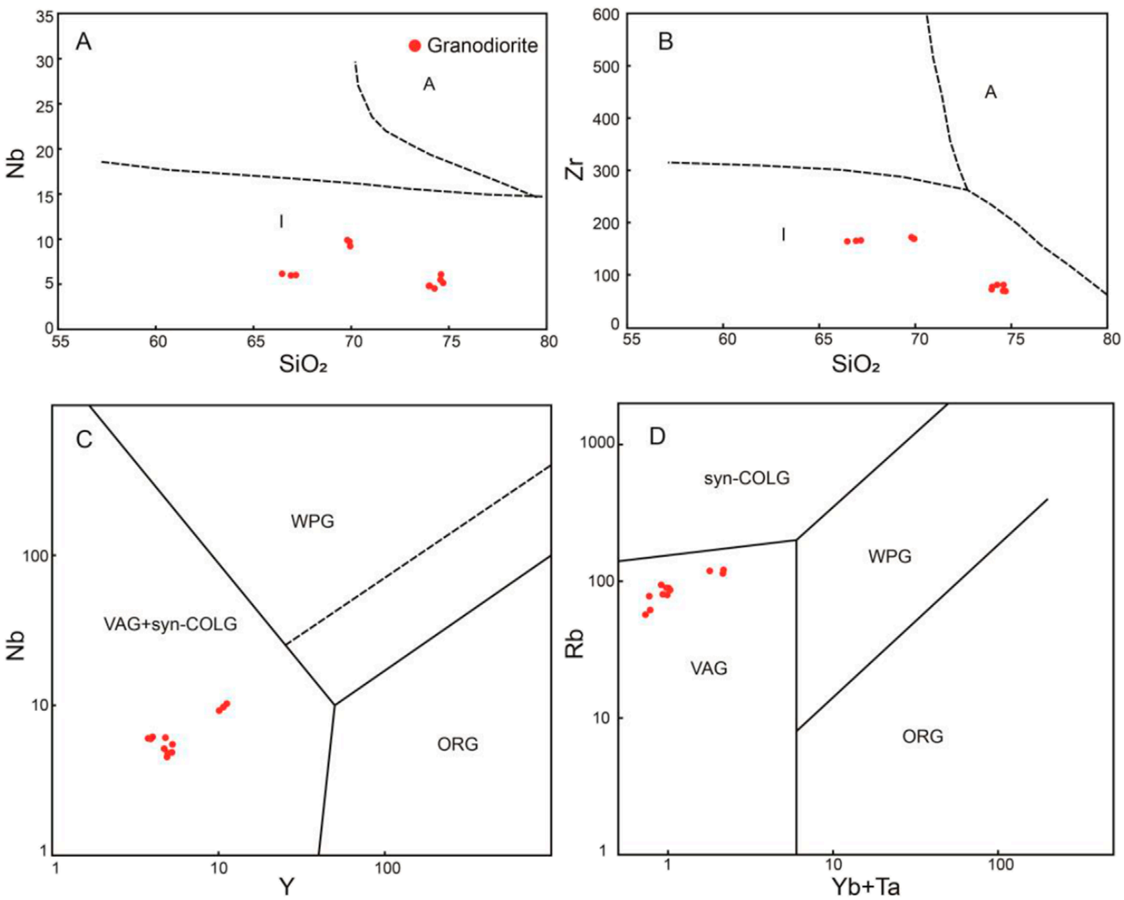

FIGURE 17
Discrimination diagrams for A-type and I-type granites and their tectonic environments: **(A)** Nb-SiO2 discrimination diagram (Collins et al., 1982); **(B)** Zr-SiO2 discrimination diagram (Collins et al., 1982); **(C)** Nb-Y discrimination diagram (Pearce et al., 1984) **(D)** Rb-(Y+Ta) discrimination diagram (Pearce et al., 1984). I - I-type granite, A - A-type granite; WPG - Within Plate Granite, ORG - Ocean Ridge Granite, VAG - Volcanic Arc Granite, syn-COLG - Syn-Collision Granite.

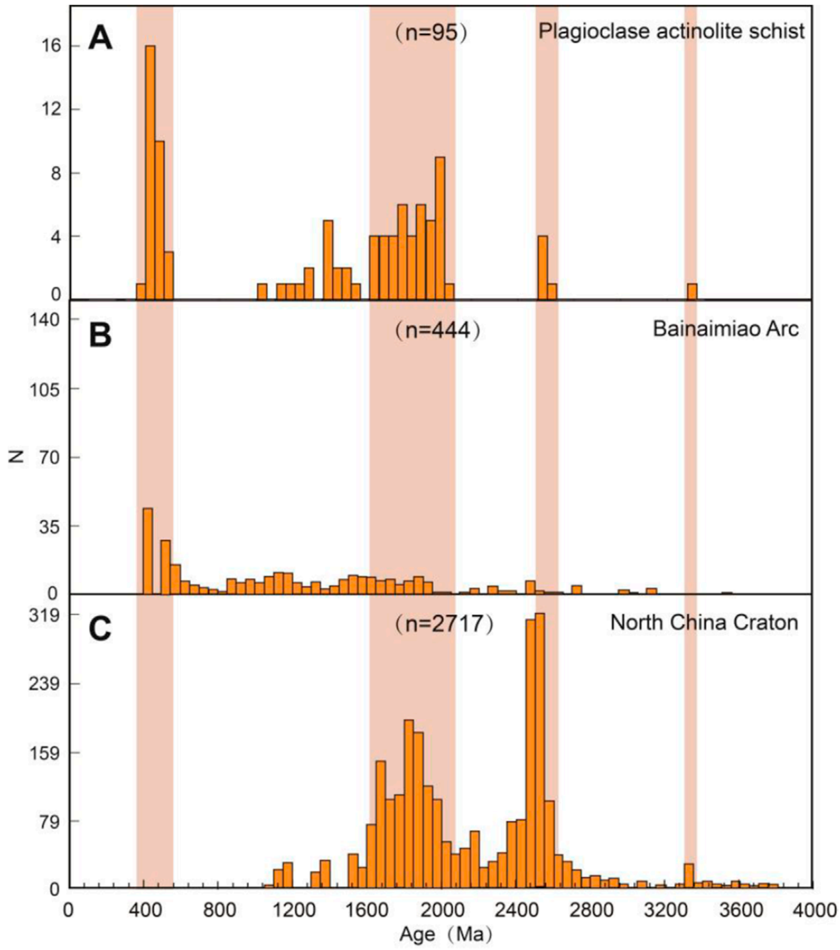

FIGURE 18
Comparison of zircon age histograms: **(A)** Plagioclase actinolite schist; **(B)** Bainaimiao arc (Zhang et al., 2014; Chen et al., 2020; Zhou et al., 2021); **(C)** North China Craton (Rojas-Agramonte et al., 2011; Wang et al., 2015; Liu et al., 2017; Zhou et al., 2021).

mélange displays two distinct age peaks (Figure 11). The younger age peak corresponds to the age of island-arc magmatic rocks, whereas the older age exhibits similarities to the NCC (Figure 18), suggesting that the plagioclase actinolite schist at this time accumulated sedimentary material from both the Bainaimiao arc and the northern margin of the NCC. The closure of the South Bainaimiao Ocean took place prior to the metamorphic age of 421 Ma for the plagioclase actinolite schist. In summary, the closure of the South Bainaimiao Ocean occurred during the Late Silurian. During this period, the Bainaimiao arc and the northern margin of the NCC underwent arc-continent collision, which continued until the conclusion of the early Devonian collisional orogeny.

5.3.3 Evolutionary process

Scholars have conducted extensive research on Early Paleozoic evolution in various regions of the Bainaimiao Arc within the South Bainaimiao Ocean and proposed several evolutionary models (Zhang et al., 2014; Chen et al., 2020; Shi et al., 2024). This study categorizes the Early Paleozoic evolution in the South Bainaimiao Ocean into three distinct stages based on the findings. The oldest rock fragments in the Chagendalai serpentinite mélange date back to 448–450 Ma (Meng et al., 2021), suggesting that the South Bainaimiao Ocean had formed. During this period, the Bainaimiao arc separated the South Bainaimiao Ocean from the Paleo-Asian Ocean, with the former serving as a branch ocean basin (Figure 19A). Ages of ophiolite blocks suggest that the South Bainaimiao Ocean persisted into the Late Middle to Late Silurian. From 450 to 424 Ma, ongoing northward subduction of the South Bainaimiao Ocean resulted in significant Bainaimiao arc-related magmatism (Figure 19B). The closure of the South Bainaimiao Ocean is dated to the Late Silurian based on ages of the matrix and the youngest blocks within the ophiolite. During this period, the ophiolite matrix accumulated sediment from both Bainaimiao arc magmatism and materials of the northern margin of the NCC. The Bainaimiao arc collided with the NCC, leading to arc-continent collision (Figure 19C). Following the arc-continent collision in the Late Silurian, a composite the NCC and the Bainaimiao arc emerged south of the Solon Suture Zone. Hence, arc-continent collision in the CAOB was pivotal in its formation and the growth of continental crust (Zhang et al., 2014). Subsequently, the NCC and the Bainaimiao arc remained a passive continental margin until the Late Carboniferous to Middle Permian, when southward subduction of Paleozoic South Asia transformed it into an Andean-type active continental margin (Song et al., 2021; Li et al., 2023; Li et al., 2023).

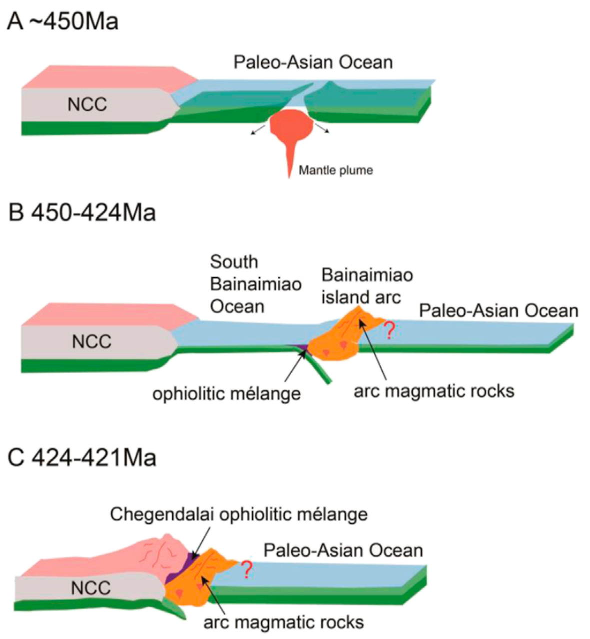

FIGURE 19
Early Paleozoic evolution of the South Bainaimiao Ocean (Zhang et al., 2014; Shi et al., 2024).

6 Conclusion

(1) This study determined the following ages: Plagioclase actinolite schist, which forms the matrix of the ophiolitic mélange, is dated at 421 Ma; ultrabasic rock blocks are dated at 424 Ma; diabase porphyrite blocks have an age of 431.9 Ma; tonalite has a zircon U-Pb age of 425.7 Ma; and granodiorite has zircon U-Pb ages of 431 Ma and 433.2 Ma.

(2) Gabbros and ultrabasic rocks derived from the lithospheric mantle and undergo assimilation and mixing with the crust. Tonalite, quartz diorite, and granodiorite are island arc magmatic rocks formed by the interaction of subducted slabs, melting, the mantle wedge, and the crust, and exhibit geochemical characteristics similar to adakites. The gabbro and ultrabasic rocks in this study may be associated with tectonic environments such as volcanic arc basalt or mid-ocean ridges. The magmatic rocks in the northern part of Damaoqi are associated with a volcanic island arc tectonic environment.

(3) The evolution of the South Bainaimiao Ocean is divided into three stages: First stage (~450 Ma): The Bainaimiao arc separated the South Bainaimiao Ocean from the Paleo-Asian Ocean, with the former acting as a branch basin of the latter. Second stage (450–424 Ma): The South Bainaimiao Ocean subducted northward. The subducted slab partially melted and interacted with the crust-mantle wedge, producing subduction-related island arc magmatic rocks. Third stage (424–421 Ma): The South Bainaimiao Ocean closed, leading to an arc-continent collision between the Bainaimiao arc and the northern margin of the North China Craton.

Data availability statement

The original contributions presented in the study are included in the article/supplementary material, further inquiries can be directed to the corresponding author.

Author contributions

Chenfei Feng: Data curation, Investigation, Methodology, Visualization, Writing–original draft. GW: Conceptualization, Funding acquisition, Investigation, Project administration, Resources, Writing–review and editing. ZZ: Conceptualization, Funding acquisition, Investigation, Project administration, Resources, Writing–review and editing. SG: Writing–review and editing. JC: Investigation, Writing–review and editing. HH: Investigation, Writing–review and editing.

Funding

The author(s) declare that financial support was received for the research, authorship, and/or publication of this article. This research was financially supported by the National Science Foudation of China: Early Paleozoic tectonic framework and evolution in the southern margin of western Xing-Meng Orogenic Belt (42272239) and The spatial-temporal relationships and its tectonic significance of the newly discovered tectonic mélange within the Xingmeng Orogenic Belt (41872232).

Conflict of interest

The reviewer JW declared a shared affiliation with the authors to the handling editor at the time of review.

The authors declare that the research was conducted in the absence of any commercial or financial relationships that could be construed as a potential conflict of interest.

Publisher's note

Supplementary material

The Supplementary Material for this article can be found online at: https://www.frontiersin.org/articles/10.3389/feart.2024.1487090/full#supplementary-material

References

Alexis N'dri, K., Zhang, D., Zhang, T., Soh Tamehe, L., Serge Kouamelan, K., Wu, M., et al. (2021). Gold mineralization in the northern margin of the North China Craton: influence of alkaline magmatism and regional tectonic during Middle Paleozoic-Mesozoic. *Ore Geol. Rev.* 133, 103969. doi:10.1016/j.oregeorev.2020.103969

Alvarez-Marron, J., Brown, D., Perez-Estaun, A., Puchkov, V., and Gorozhanina, Y. (2000). Accretionary complex structure and kinematics during Paleozoic arc–continent collision in the southern Urals. *Tectonophysics* 325, 175–191. doi:10.1016/s0040-1951(00)00136-0

Atherton, M. P., and Petford, N. (1993). Generation of sodium-rich magmas from newly underplated basaltic crust. *Nature* 362, 144–146. doi:10.1038/362144a0

Barbarin, B. (1999). A review of the relationships between granitoid types, their origins and their geodynamic environments. *Lithos* 46, 605–626. doi:10.1016/s0024-4937(98)00085-1

Brown, D., Spadea, P., Puchkov, V., Alvarez-Marron, J., Herrington, R., Willner, A. P., et al. (2006). Arc–continent collision in the southern Urals. *Earth-Science Rev.* 79, 261–287. doi:10.1016/j.earscirev.2006.08.003

Chen, W., Zhiguang, Z., Andrew, V. Z., Guosheng, W., Changfeng, L., and Tian, J. (2018). A 1.9-Ga mélange along the Northern margin of the North China craton: implications for the assembly of columbia supercontinent. *Tectonics* 37, 3610–3646. doi:10.1029/2018tc005103

Chen, Y., Zhang, Z. C., Qian, X., Li, J., Ji, Z. J., and Wu, T. (2020). Early to mid-Paleozoic magmatic and sedimentary records in the Bainaimiao Arc: an advancing subduction-induced terrane accretion along the northern margin of the North China Craton. *Gondwana Res.* 79, 263–282. doi:10.1016/j.gr.2019.08.012

Chen, Y. C., Zhang, J. E., Hou, Q. L., Yan, Q. R., and Xiao, W. J. (2021). The basic characteristics of accretion arcs and its geological implications. *Chin. J. Geology (Scientia Geol. Sinica)* 56, 615–634. doi:10.12017/dzkx.2021.031

Collins, W. J., Beams, S. D., White, A. J. R., and Chappell, B. W. (1982). Nature and origin of A-type granites with particular reference to southeastern Australia. *Contributions Mineralogy Petrology* 80, 189–200. doi:10.1007/bf00374895

Defant, M. J., and Drummond, M. S. (1990). Derivation of some modern arc magmas by melting of young subducted lithosphere. *Nature* 347, 662–665. doi:10.1038/347662a0

Degtyarev, K. E., and Ryazantsev, A. V. (2007). Cambrian arc-continent collision in the Paleozoides of Kazakhstan. *Geotectonics* 41, 63–86. doi:10.1134/s0016852107010062

Drummond, M. S., and Defant, M. J. (1990). A model for Trondhjemite-Tonalite-Dacite Genesis and crustal growth via slab melting: Archean to modern comparisons. *J. Geophys. Res. Solid Earth* 95, 21503–21521. doi:10.1029/jb095ib13p21503

Gu, C. N., Zhou, Z. G., Zhang, Y. K., Liu, C. F., Liu, W. C., and Yu, Y. S. (2012). Zircon dating of the baiyinduxi Group in inner Mongolia and lts tectonic interpretation. *Geoscience* 26, 1–9.

Hao, Y., Wen-Chun, G., Santosh, M., Zheng, J., Yu, D., Yan, J., et al. (2022). The role of continental fragments in the formation of intra-oceanic arcs: constraints from Sr-Nd-Hf-O isotopes of gabbro from the Jiamusi Block, NE China. *Gondwana Res.* 103, 297–313. doi:10.1016/j.gr.2021.10.009

Hofmann, A. W. (1988). Chemical differentiation of the Earth: the relationship between mantle, continental crust, and oceanic crust. *Earth Planet. Sci. Lett.* 90, 297–314. doi:10.1016/0012-821x(88)90132-x

Hou, L. Y., Zhang, C. H., Lin, Y., Li, C. M., Huang, Y. Z., Dong, T., et al. (2020). From oblique arc-continent collision to orthogonal plate subduction in the southeastern central Asia Orogenic Belt during Paleozoic: evidence from superimposed folds at the northern margin of the north China Craton. *J. Asian Earth Sci.* 200, 104499. doi:10.1016/j.jseaes.2020.104499

Hu, X. J., Yang, Z. L., Wang, S. Q., Zhao, L. G., Wang, W. L., Li, M., et al. (2022). Geochronology and geochemistry of the Early Paleozoic volcanic rocks from the Baoerhantu arc in lnnerMongolia: petrogenesis and constraints on the tectonic evolution of the Xing-Meng orogenic belt. *Acta Geol. Sin.* 96, 897–917. doi:10.19762/j.cnki.dizhixuebao.2021155

Huang, S., and Frey, F. A. (2003). Trace element abundances of Mauna Kea basalt from phase 2 of the Hawaii Scientific Drilling Project: petrogenetic implications of correlations with major element content and isotopic ratios. *Geochem. Geophys. Geosystems* 4. doi:10.1029/2002gc000322

Irvine, T. N., and Baragar, W. R. A. (1971). A guide to the chemical classification of the common volcanic rocks. *Can. J. Earth Sci.* 8, 523–548. doi:10.1139/e71-055

Jia, H. Y., Bao, Y., and Zhang, Y. Q. (2003). *Characteristics and tectonic significance of the Wude suture zone in northern Damaoqi, Inner Mongolia*. Journal of Chengdu University of Technology (Science and Technology Edition, 30–34.

Johnson, C., Amory, J., Zinniker, D., Lamb, M., Graham, S. A., Affolter, M., et al. (2007). Sedimentary response to Arc-Continent collision, permian, southern Mongolia. *AGU Fall Meet. Abstr.* 436. doi:10.1130/2008.2436(16)

Kieffer, B., Arndt, N., Lapierre, H., Bastien, F., Bosch, D., Pecher, A., et al. (2004). Flood and shield basalts from Ethiopia: magmas from the African superswell. *J. Petrology* 45, 793–834. doi:10.1093/petrology/egg112

Konstantinovskaya, E. (2011). "Early eocene arc–continent collision in kamchatka, Russia: structural evolution and geodynamic model," in *Arc-continent collision*. Editors D. Brown, and P. D. Ryan (Berlin, Heidelberg: Springer Berlin Heidelberg).

Kröner, A., Kovach, V., Belousova, E., Hegner, E., Armstrong, R., Dolgopolova, A., et al. (2014). Reassessment of continental growth during the accretionary history of the central asian orogenic belt. *Gondwana Res.* 25, 103–125. doi:10.1016/j.gr.2012.12.023

Li, J. L. (2004). Basic characteristics of accretion-type orogens. *Geol. Bull. China*, 947–951.

Li, J. L., Wu, C., Cheng, L., Yang, H., Zhu, D. C., and Liu, J. G. (2023). Geodynamic controls on the Paleo-Asian oceanic plate evolution: constraints from Paleozoic intrusive suites along the northern margin of the North China Block. *Lithos* 454-455, 107258. doi:10.1016/j.lithos.2023.107258

Li, J. Y., Zhang, J., Yang, T. N., Li, Y. P., Sun, G. H., Zhu, Z. X., et al. (2009). Crustal tectonic division and evolution of the southern part of theNorth asian orogenic region and its adjacent areas. *J. Jilin Univ. Sci. Ed.* 39, 584–605. doi:10.13278/j.cnki.jjuese.2009.04.008

Li, P. Q., Song, D. F., and Zeng, H. (2023). Late Carboniferous arc-continent collision and subduction polarity reversal in southeast Altaids: new insights from provenance analysis of late Paleozoic sedimentary records. *J. Asian Earth Sci.* 248, 105616. doi:10.1016/j.jseaes.2023.105616

Li, S., Wang, T., Xiao, W. J., and Hou, Q. L. (2023). Tectono-magmatic evolution from accretion to collision in the southern margin of the Central Asian Orogenic Belt. *Acta Petrol. Sin.* 39, 1261–1275. doi:10.18654/1000-0569/2023.05.03

Li, W. B., Hu, C. S., Zhong, R., and Zhu, F. (2015). U–Pb, 39Ar/40Ar geochronology of the metamorphosed volcanic rocks of the Bainaimiao Group in central Inner Mongolia and its implications for ore genesis and geodynamic setting. *J. Asian Earth Sci.* 97, 251–259. doi:10.1016/j.jseaes.2014.06.007

Li, W. B., Zhong, R., Xu, C., Song, B., and Qu, W. J. (2012). U–Pb and Re–Os geochronology of the Bainaimiao Cu–Mo–Au deposit, on the northern margin of the North China Craton, Central Asia Orogenic Belt: implications for ore genesis and geodynamic setting. *Ore Geol. Rev.* 48, 139–150. doi:10.1016/j.oregeorev.2012.03.001

Liu, C. F., Liu, W. C., Wang, H. P., Zhou, Z. G., Zhang, H. F., and Tang, Y. J. (2014). Geochronology and geochemistry of the Bainaimiao metavolcanic rocks in the northern margin of north China craton. *Acta Geol. Sin.* 88, 1273–1287.

Liu, C. H., Zhao, G. C., Liu, F. L., and Shi, J. R. (2017). Detrital zircon U-Pb and Hf isotopic and whole-rock geochemical study of the Bayan Obo Group, northern margin of the North China Craton: implications for Rodinia reconstruction. *Archean Proterozoic Evol. North China Craton* 303, 372–391. doi:10.1016/j.precamres.2017.04.033

Liu, J. F., Li, J. Y., Chi, X. G., Feng, Q. W., Hu, Z. C., and Zhou, K. (2013). Early Devonian felsic volcanic rocks related to the arc-continent colision on the northern margin of North China craton-evidences of zircon U-Pb dating and geochemical characteristics. *Geol. Bull. China* 32, 267–278.

Liu, M., Lai, S. C., Zhang, D., Zhu, R. Z., Qin, J. F., Xiong, G. Q., et al. (2020). Constructing the latest neoproterozoic to early paleozoic multiple crust-mantle interactions in western Bainaimiao arc terrane, southeastern central asian orogenic belt. *Geosci. Front.* 11, 1727–1742. doi:10.1016/j.gsf.2020.01.012

Ludwig, K. R. (2003). *Isoplot 3.00: a geochronological toolkit for microsoft excel*. Berkeley Geochronology Center Special Publication, 70.

Ma, C., Tang, Y. J., and Ying, J. F. (2019). Magmatism in subduction zones and growth of continental crust. *Earth Sci.* 44, 1128. doi:10.3799/dqkx.2019.026

Ma, H. T., Ma, X., Chen, J. F., Chen, B., Li, C., Zhou, L. M., et al. (2020). The zhangjiatun igneous complex in the southeastern margin of the central asian orogenic belt, NE China: evidence for an early paleozoic intra-oceanic arc. *Sedimentology, Geodyn. Resour. Environ. China adjacent Areas* 194, 104182. doi:10.1016/j.jseaes.2019.104182

Ma, S. X., Wang, Z. Q., Zhang, Y., and Sun, J. X. (2019). Bainaimiao Arc as an exotic terrane along the Northern margin of the North China craton: evidences from petrography, zircon U-Pb dating, and geochemistry of the early devonian deposits. *Tectonics* 38, 2606–2624. doi:10.1029/2018tc005426

Ma, Y. L., Zhong, Y., Furnes, H., Zhaxi, Q. B., Pang, J. H., Liu, W. L., et al. (2021). Origin and tectonic implications of boninite dikes in the Shiquanhe ophiolite, western Bangong Suture, Tibet. *J. Asian Earth Sci.* 205, 104594. doi:10.1016/j.jseaes.2020.104594

Maniar, P. D., and Piccoli, P. M. (1989). Tectonic discrimination of granitoids. *GSA Bull.* 101, 635–643. doi:10.1130/0016-7606(1989)101<0635:tdog>2.3.co;2

Martin, H. (1986). Effect of steeper Archean geothermal gradient on geochemistry of subduction-zone magmas. *Geology* 14, 753–756. doi:10.1130/0091-7613(1986)14<753:eosagg>2.0.co;2

Martin, H. (1999). Adakitic magmas: modern analogues of Archaean granitoids. *Lithos* 46, 411–429. doi:10.1016/s0024-4937(98)00076-0

Meng, Y. X., Zhang, Z. C., Tang, J. Z., Zhang, H. H., Wang, Q., and Ding, C. (2021). Late Ordovician fore-arc ophiolitic mélange in the southern margin of the Bainaimiao arc: constraints from zircon U–Pb–Hf isotopes and geochemical analyses. *Geol. Mag.* 158, 2042–2062. doi:10.1017/s0016756821000662

Middlemost, E. A. K. (1994). Naming materials in the magma/igneous rock system. *Earth-Science Rev.* 37, 215–224. doi:10.1016/0012-8252(94)90029-9

Pearce, J. A. (1982). Trace element characteristics of lavas from destructive plate boundaries. *Andesites Orogenic Andesites Relat. Rocks*, 525–548. doi:10.1016/j.lithos.2020.105567

Pearce, J. A., Harris, N. B., and Tindle, A. G. (1984). Trace element discrimination diagrams for the tectonic interpretation of granitic rocks. *J. Petrology* 25, 956–983. doi:10.1093/petrology/25.4.956

Pearce, J. A., and Robinson, P. T. (2010). The Troodos ophiolitic complex probably formed in a subduction initiation, slab edge setting. *A Tribute Miyashiro* 18, 60–81. doi:10.1016/j.gr.2009.12.003

Qian, X., Zhang, Z., Chen, Y., Yu, H., Luo, Z., and Yang, J. (2017). Geochronology and geochemistry of early paleozoic igneous rocks in zhurihe area, inner Mongolia and their tectonic significance. *Diqiu Kexue - Zhongguo Dizhi Daxue Xuebao/Earth Sci. - J. China Univ. Geosciences* 42, 1472–1494. doi:10.3799/dqkx.2017.545

Rojas-Agramonte, Y., Kröner, A., Demoux, A., Xia, X., Wang, W., Donskaya, T., et al. (2011). Detrital and xenocrystic zircon ages from Neoproterozoic to Palaeozoic arc terranes of Mongolia: significance for the origin of crustal fragments in the Central Asian Orogenic Belt. *Isl. Arcs Their role growth accretionary orogens mineral Endow.* 19, 751–763. doi:10.1016/j.gr.2010.10.004

Safonova, I., Seltmann, R., Kröner, A., Gladkochub, D., Kim, J.-Y., Schulmann, K., et al. (2011). A new concept of continental construction in the central asian orogenic belt: (compared to actualistic examples from the western pacific). *Episodes* 34, 1–10. doi:10.18814/epiiugs/2011/v34i3/005

Saunders, A. D., Storey, M., Kent, R. W., and Norry, M. J. (1992). *Consequences of plume-lithosphere interactions*. London, Special Publications: Geological Society, 41–60.

Şengör, A. M. C., Natal'in, B. A., and Burtman, V. S. (1993). Evolution of the Altaid tectonic collage and Palaeozoic crustal growth in Eurasia. *Nature* 364, 299–307. doi:10.1038/364299a0

Shi, Y., Wen, K., Santosh, M., Zhang, C., Li, N., Su, W., et al. (2024). The role of intra-oceanic arc in the growth of continental crust: evidence from the Early Paleozoic Bainaimiao arc. *Gondwana Res.* 131, 256–277. doi:10.1016/j.gr.2024.03.005

Shi, Y. R., Liu, D. Y., Miao, L. C., Zhang, F. Q., Jian, P., Zhang, W., et al. (2010). Devonian A-type granitic magmatism on the northern margin of the North China Craton: SHRIMP U–Pb zircon dating and Hf-isotopes of the Hongshan granite at Chifeng, Inner Mongolia, China. *Gondwana Res.* 17, 632–641. doi:10.1016/j.gr.2009.11.011

Smith, A. G., and Rassios, A. (2003). *The evolution of ideas for the origin and emplacement of the western Hellenic ophiolites*. Special papers-geological society of america, 337–350.

Smith, E. I., Sánchez, A., Walker, J. D., and Wang, K. (1999). Geochemistry of mafic magmas in the hurricane volcanic field, Utah: implications for small- and large-scale chemical variability of the lithospheric mantle. *J. Geol.* 107, 433–448. doi:10.1086/314355

Song, D. F., Xiao, W. J., Windley, B. F., Mao, Q. g., Ao, S. J., Wang, H. Y. C., et al. (2021). Closure of the Paleo-Asian Ocean in the middle-late triassic (Ladinian-Carnian): evidence from provenance analysis of retroarc sediments. *Geophys. Res. Lett.* 48, e2021GL094276. doi:10.1029/2021gl094276

Stern, C. R., and Kilian, R. (1996). Role of the subducted slab, mantle wedge and continental crust in the generation of adakites from the Andean Austral Volcanic Zone. *Contributions Mineralogy Petrology* 123, 263–281. doi:10.1007/s004100050155

Sun, S. S., and McDonough, W. F. (1989) Chemical and isotopic systematics of oceanic basalts: implications for mantle composition and processes. *Geological Society, London, Special Publications* 42 (1), 313–345. doi:10.1144/gsl.sp.1989.042.01.19

Tang, J. Z., Zhang, Z. C., Xue, J. Z., Liu, B., Chen, Y., and Zhang, S. H. (2021). Permo-Carboniferous provenance shifts at the northern margin of the North China Craton and their tectonic implications: detrital zircon U–Pb–Hf records from central Inner Mongolia. *Gondwana Res.* 95, 134–148. doi:10.1016/j.gr.2021.03.012

Tao, J. X., Xu, L. Q., He, F., and Su, M. R. (2005). Petrological evidence for subduction of the early paleozoic oceanic crust in bart - Obo, inner Mongolia. *North China Geol.*, 1–8.

Tian, R., Wang, X., Ge, R., Zhu, W., and Xie, G. (2023). Early to Middle Paleozoic magmatism and metamorphism in the Alxa Block and its northern margin: implications for the western extension of the Bainaimiao arc. *Lithos* 440-441, 107041. doi:10.1016/j.lithos.2023.107041

Vermeesch, P. (2012). On the visualisation of detrital age distributions. *Chem. Geol.* 312-313, 190–194. doi:10.1016/j.chemgeo.2012.04.021

Wang, J., Meng, X., Chen, Z., Liu, G., Zheng, Y., Wang, J., et al. (2015). Lithologic mapping test for gravity and magnetic anomalies: a case study of gravity–magnetic anomaly profile in the eastern segment of the China–Mongolia border. *J. Appl. Geophys.* 117, 23–31. doi:10.1016/j.jappgeo.2015.03.020

Wang, Q. F., Deng, J., Liu, X. F., Zhao, R., and Cai, S. H. (2016). Provenance of Late Carboniferous bauxite deposits in the North China Craton: new constraints on marginal arc construction and accretion processes. *Gondwana Res.* 38, 86–98. doi:10.1016/j.gr.2015.10.015

Wang, S., Zhang, S. H., Zhang, Q. Q., Liang, X., Kong, L. H., Hu, G. H., et al. (2022). *In-situ* zircon U-Pb dating method by LA-CP-MS and discussions on the effect of different beam spot diameters on the dating results. *J. Geomechanics* 28, 642–652.

Whattam, S. A. (2009). Arc-continent collisional orogenesis in the SW Pacific and the nature, source and correlation of emplaced ophiolitic nappe components. *Mantle Dyn. Crust-Mantle Interact. Collisional Orogens* 113, 88–114. doi:10.1016/j.lithos.2008.11.009

Windley, B. F., Alexeiev, D., Xiao, W., Kröner, A., and Badarch, G. (2007). Tectonic models for accretion of the central asian orogenic belt. *J. Geol. Soc.* 164, 31–47. doi:10.1144/0016-76492006-022

Wood, D. A. (1980). The application of a ThHfTa diagram to problems of tectonomagmatic classification and to establishing the nature of crustal contamination of basaltic lavas of the British Tertiary Volcanic Province. *Earth Planet. Sci. Lett.* 50, 11–30. doi:10.1016/0012-821x(80)90116-8

Wu, C., Liu, C. F., Zhu, Y., Zhou, Z. G., Jiang, T., Wencan, L., et al. (2016). Early paleozoic magmatic history of central inner Mongolia, China: implications for the tectonic evolution of the southeast central asian orogenic belt. *Int. J. Earth Sci.* 105, 1307–1327. doi:10.1007/s00531-015-1250-7

Xiao, W. J., Song, D. F., Mao, Q. G., Wan, B., Zhang, J. E., Ao, S. J., et al. (2022). How to effectively determine the time limit of accretion orogeny. *Earth Sci.* 47, 3770. doi:10.3799/dqkx.2022.802

Xiao, W. J., Windley, B. F., Hao, J., and Zhai, M. G. (2003). Accretion leading to collision and the Permian Solonker suture, Inner Mongolia, China: termination of the central Asian orogenic belt. *Tectonics* 22. doi:10.1029/2002tc001484

Xu, B., Charvet, J., Chen, Y., Zhao, P., and Shi, G. Z. (2013). Middle Paleozoic convergent orogenic belts in western Inner Mongolia (China): framework, kinematics, geochronology and implications for tectonic evolution of the Central Asian Orogenic Belt. *Gondwana Res.* 23, 1342–1364. doi:10.1016/j.gr.2012.05.015

Xu, B., and Chen, B. (1997). Framework and evolution of the middle paleozoic orogenic belt between siberian and north China plates in northern inner Mongolia. *Sci. China Ser. D Earth Sci.* 40, 463–469. doi:10.1007/bf02877610

Xu, L. Q., Deng, J. F., Chen, Z. Y., and Tao, J. X. (2003). The identification of ordovician adakites and its significant in northern Damao, inner Mongolia. *Geoscience*, 428–434.

Yang, Z. L., Liu, Y., Teng, F., Wang, W. L., Hu, X. J., Guo, S., et al. (2019). Geochronology and geochemistry of the early paleozoic volcanic rocks in eastern segment of the Bainaimiao Arc, and their geological sianificances. *Geol. J. China Univ.* 25, 206–220. doi:10.16108/j.issn1006-7493.2018111

Yuan, S. H., Pan, G. T., Wang, L. Q., Jiang, X. S., Yin, F. G., Zhang, W. P., et al. (2009). Accretionary orogenesis in the active continental margins. *Earth Sci. Front.* 16, 31–48. doi:10.1016/s1872-5791(08)60095-0

Zeng, H., Song, D. F., Xiao, W. J., and Li, P. Q. (2023). Accretion of an early Paleozoic Alaska-type arc onto northern North China: implications for continental growth of the Central Asian orogenic belt. *GSA Bull.* doi:10.1130/b36594.1

Zhang, J. F., Liu, Z. H., Guan, Q. B., Xu, Z. Y., Wang, X. A., and Zhu, K. (2017). Age and geological significance of Xuniwusu Formation from bainaimia area of sonid youqi, inner Mongolia. *Acta Petrol. Sin.* 33, 3147–3160.

Zhang, J. R., Wei, C. J., and Chu, H. (2018). New model for the tectonic evolution of Xing'an-lnner Mongolia Orogenic Belt:Evidence from four different oases of metamorphism in Centralinner Mongolia. *Acta Petrol. Sin.* 34, 2857–2872.

Zhang, Q. Q., Zhang, S. H., Zhao, Y., and Hu, G. H. (2024). Compositionally variable basement and tectonic affinity of the Bainaimiao arc belt: implications for crustal growth of the Central Asian Orogenic Belt. *J. Asian Earth Sci.* 263, 106009. doi:10.1016/j.jseaes.2024.106009

Zhang, Q. Q., Zhang, S. H., Zhao, Y., and Liu, J. M. (2018). Devonian alkaline magmatic belt along the northern margin of the North China Block: petrogenesis and tectonic implications. *Lithos* 302-303, 496–518. doi:10.1016/j.lithos.2018.01.019

Zhang, S. H., Zhao, Y., Li, X. H., Ernst, R. E., and Yang, Z. Y. (2017). The 1.33–1.30 Ga yanliao large igneous province in the North China craton: implications for reconstruction of the nuna (columbia) supercontinent, and specifically with the North Australian craton. *Earth Planet. Sci. Lett.* 465, 112–125. doi:10.1016/j.epsl.2017.02.034

Zhang, S. H., Zhao, Y., Ye, H., Liu, J. M., and Hu, Z. C. (2014). Origin and evolution of the Bainaimiao arc belt: implications for crustal growth in the southern Central Asian orogenic belt. *Geol. Soc. Am. Bull.* 126, 1275–1300. doi:10.1130/b31042.1

Zhang, W., and Jian, P. (2008). SHRlMP dating of early paleozoic granites from north Damao, Inner Mongolia. *Acta Geol. Sin.*, 778–787.

Zhang, W., Jian, P., Kröner, A., and Shi, Y. (2013). Magmatic and metamorphic development of an early to mid-Paleozoic continental margin arc in the southernmost Central Asian Orogenic Belt, Inner Mongolia, China. *J. Asian Earth Sci.* 72, 63–74. doi:10.1016/j.jseaes.2012.05.025

Zhang, X. H., Zhang, H. F., Jiang, N., Zhai, M. G., and Zhang, T. B. (2010). Early Devonian alkaline intrusive complex from the northern North China craton: a petrological monitor of post-collisional tectonics. *J. Geol. Soc.* 167, 717–730. doi:10.1144/0016-76492009-110

Zhang, Y. Q., Meng, E. G., Gong, Z. Z., Han, J. G., and Wang, T. (2004). Division and age of the mid-upper silurian Xibiehe Formation in central inner Mongolia. *Geol. Bull. China* 23, 352–359.

Zhang, Y. Q., Zhang, Y. Q., Luo, Z. Z., Bai, Y. L., and Bai, B. (2020). LA-MC-ICP-MS U-Pb dating of zircons from the Meta-Andesites in the Bainaimiao Formation in the Bainaimiao copper mine, inner Mongolia. *J. Stratigr.* 44, 207–214. doi:10.19839/j.cnki.dcxzz.2020.0022

Zhao, P., Chen, Y., Xu, B., Faure, M., Shi, G., and Choulet, F. (2013). Did the Paleo-Asian Ocean between North China block and Mongolia block exist during the late Paleozoic? First paleomagnetic evidence from central-eastern Inner Mongolia, China. *J. Geophys. Res. Solid Earth* 118, 1873–1894. doi:10.1002/jgrb.50198

Zhou, H., Zhao, G. C., Han, Y. G., and Wang, B. (2018). Geochemistry and zircon U-Pb-Hf isotopes of Paleozoic intrusive rocks in the Damao area in Inner Mongolia, northern China: implications for the tectonic evolution of the Bainaimiao arc. *Lithos* 314-315, 119–139. doi:10.1016/j.lithos.2018.05.020

Zhou, H., Zhao, G. C., Han, Y. G., Wang, B., and Pei, X. Z. (2021). Tectonic origin of the Bainaimiao arc terrane in the southern Central Asian orogenic belt: evidence from sedimentary and magmatic rocks in the Damao region. *GSA Bull.* 133, 802–818. doi:10.1130/b35496.1

Zhou, Z. G., Hu, M. M., Wu, C., Wang, G. S., Liu, C. F., Cai, A., et al. (2018a). Coupled U–Pb dating and Hf isotopic analysis of detrital zircons from Bayan Obo Group in Inner Mongolia: constraints on the evolution of the Bayan Obo rift belt. *Geol. J.* 53, 2649–2664. doi:10.1002/gj.3102

Zhou, Z. G., Zhang, D., Gu, Y. C., Wang, G. S., Li, H. Y., Yu, Y. S., et al. (2018b). Characteristics of Bainaimiao thrust belt along central lnner Mongolia in north China and its geological significance. *Geotect. Metallogenia* 42, 1–17. doi:10.16539/j.ddgzyckx.2018.01.001

Zhou, Z. H., Mao, J. W., Ma, X. H., Che, H. W., Ou'yang, H. G., and Gao, X. (2017). Geochronological framework of the early Paleozoic Bainaimiao Cu-Mo-Au deposit, NE China, and its tectonic implications. *East. Central Asian Orogenic Belt Form. Evol.* 144, 323–338. doi:10.1016/j.jseaes.2016.11.005